NMSCAA'26

5th INTERNATIONAL CONFERENCE ON NUMERICAL METHODS FOR SCIENTIFIC COMPUTATIONS AND ADVANCED APPLICATIONS

June 15–18, 2026

Sozopol, Bulgaria

ABSTRACTS AND SHORT COMMUNICATIONS

SVETOZAR MARGENOV

INTERNATIONAL CONFERENCE

NMSCAA'26

SOZOPOL, BULGARIA
JUNE 15 – 18, 2026

NUMERICAL METHODS FOR SCIENTIFIC COMPUTATIONS AND ADVANCED APPLICATIONS

PROCEEDINGS
OF SHORT COMMUNICATIONS

SVETOZAR MARGENOV

Editor
Svetozar Margenov
Bulgarian Academy of Sciences
Sofia, Bulgaria

ISBN 978-619-7320-11-4 (eBook)
Institute of Information and Communication Technologies, Bulgarian Academy of Sciences,
Acad. G. Bonchev Str., Bl. 2, 1113 Sofia, Bulgaria, 2026

PREFACE

The 5th International Conference on Numerical Methods for Scientific Computations and Advanced Applications (NMSCAA'26) is organized by the Institute of Information and Communication Technologies, Bulgarian Academy of Sciences and MIV Consult Ltd. in cooperation with Bulgarian Section of SIAM (BG SIAM).

Traditionally, the main thematic areas of NMSCAA'26 include: (i) modeling, simulation, and optimization; (ii) multiscale and multiphysics problems; (iii) robust iterative methods and sparse matrix computations; (iv) fractional differential equations and non-local problems; (v) parallel numerical methods and scalable algorithms; and (vi) advanced applications in science and engineering.

In addition, the scientific program of the present conference features contributions addressing emerging trends, including the synergy between large-scale scientific computing and artificial intelligence techniques, novel approaches to numerical linear algebra that combine rigorous mathematical frameworks with basis reduction methods, hybrid methodologies integrating high-performance computing and quantum algorithms, as well as advanced developments in multiscale and multiphysics modeling and applications.

The purpose of the conference is to bring together researchers in the field of numerical methods for scientific computing, working on models arising in the natural sciences, as well as biomedical, environmental, and industrial applications, together with developers of algorithms for modern high-performance computing architectures. The success of the conference has been ensured by the active participation of authors from numerous countries across the world, including America, Asia, and Europe.

Svetozar Margenov

Table of Contents

J. Bannister, D. Hewett, A. Gibbs
Accurate and Efficient Numerical Methods for Acoustic Scattering by Self-Similar Fractal Inhomogeneities **1**

H. Bansu, S. Margenov
Numerical Solution of Time Fractional Black–Scholes Equation using Radial Basis Functions and Chebyshev Polynomial Collocation Method **4**

H. Chervenkov, K. Slavov
Bias Correction of EURO-CORDEX High-Resolution Simulations: Evaluation on the Near Past Climate over Southeast Europe **5**

M. Chwastyk
Numerical Modeling Strategies for Intrinsically Disordered Protein Aggregation Mechanisms **7**

H. Djidjev
Extending Quantum Annealing to Continuous Optimization **8**

A. Draganescu, B. Sousedik, S. Alzuhairy
Multilevel Methods for Optimal Control of Elliptic Equations with Stochastic Coefficients Discretized Using Stochastic Collocation **9**

S. Fidanova, N. Bozakova, V. Ivanov
Medical Sorting of Earthquake Victims **9**

S. Fidanova, N. Bozakova, M. Shopov, V. Ivanov
The Condition of a Cow Farm After an Earthquake **10**

N. Ilieva, P. Petkov, E. Lilkova, and L. Litov
Informed Strategy for Targeted Therapeutics Design **11**

S. Fidanova, V. Ivanov, N. Bozakova
Predicting Eathquaqe Using Cows as a Biosensors **12**

S. Harizanov, S. Margenov
Exploring Maximum Principles in Fractional Diffusion-Reaction Equations **13**

S. Harizanov, D. Slavchev, N. Kosturski
Error Balancing when Solving Fractional Elliptic Equations **14**

H. Hristov, K. Dimitrov, T. Penev
Investigation of the Relationship Between Rumination Activity and Eye Temperature in Dairy Cows Under Mild Heat Stress Using Infrared Thermography **15**

V. Ivanov, I. Georgieva, G. Gadzhev
Recurrence of Cold and Frosty Conditions in RCP2.6, RCP8.5 Scenarios and Historical Climate over Bulgaria **17**

M. Koleva, L. Vulkov
Compact Finite Difference Schemes for Nonlinear Shear Wave Models in Hyperelasticity **20**

N. Kosturski, S. Margenov, Y. Vutov
Mixed Precision Non-Overlapping BURA Domain Decomposition Preconditioning **22**

N. Kopteva
Error Analysis for Higher-Order Methods for Subdiffusion Equations on Quasi-Graded Meshes **22**

S. Margenov, D. Slavchev
Anomalous Heat Diffusion in Biological Tissues: A Fractional Laplacian Approach **23**

I. Marqués-Campillo
The Frequency Landscape of Genomic Sequences Across Organisms **24**

T. Ostromsky, P. Georgiev, G. Vasilev, G, Evtimov, M. Raykovska, S.-M. Gurova
Novel Technologies for Imaging, Mapping and 3D Modeling of Underground Archaeological and Karst Objects – a Medieval Well in Greben Mountain and a Karst Complex near Karlukovo Village, West Bulgaria **24**

X. Peng
On the Stability of β-Sheet Inhibitors for PD-L1: Insights from REMD **27**

E. Panek-Chwastyk, K. Dabrowska-Zielińska
Super-Resolution Reconstruction of Satellite Data: Validation and Uncertainty Assessment for Earth Observation Applications **28**

P. Petkov
Application of Differential Topology to Matrix Analysis **28**

J. Stanchov, S. Fidanova
Proactive Fuzzy-ACO Framework for Resilient Outsourced Production **31**

J. Thacker, I. Todorov, B. Speake, M. Seaton
MolSim++: GPU Confined Particle Dynamics Project **33**

I. Todorov, M. Seaton, B. Speake
Polarised Water Model for CG DPD Simulations of RFB Electrolytes **33**

S. Zhao, J. Meng, X. Peng, J. Dai, Q. Zhao
A Unified and Automated Workflow for Multi-Scale Simulation of Covalent Protein–Ligand Complexes **34**

P. Zhivkov
RF vs. LSTM for Multi-Horizon Urban Air Quality Forecasting: A Head-to-Head Benchmark on a Calibrated Hybrid Sensor Network **35**

L. Zikatanov
Auxiliary Space Preconditioning and a Posteriori Error Estimates in Finite Element Method **37**

List of participants **38**

Accurate and Efficient Numerical Methods for Acoustic Scattering by Self-Similar Fractal Inhomogeneities

J. Bannister, D. Hewett, A. Gibbs

Introduction

The simulation of scattering by an inhomogeneity, a compact region of space in which the refractive index differs from that of a homogeneous background medium, is a classical problem in computational wave propagation [5, Chapter 8]. In practice, one often encounters inhomogeneities whose boundaries are highly non-smooth, with complex multi-scale geometric features that might be modelled more accurately using fractals. For example, the scattering of electromagnetic waves by atmospheric ice crystals plays a key role in determining the composition of clouds via imaging methods and estimating the radiation balance of the Earth for climate models [3], where such ice crystal aggregates have been observed to exhibit fractal-like structures [4, 9, 10].

The simplest model for such problems is given by the inhomogeneous Helmholtz equation

$$\Delta u^s + k^2(1+m)u^s = -f, \qquad \text{on } \mathbb{R}^n \quad (n=2,3), \tag{1}$$

where the scattered field u^s with wavenumber $k > 0$ satisfies the standard outgoing Sommerfeld radiation condition, and describes scattering of time-harmonic acoustic waves and certain polarisations of time-harmonic electromagnetic waves [8, Remark 2.1]. We assume the refractive index perturbation $m \in L^\infty\left(\mathbb{R}^2\right)$ has compact support denoted by K, which we refer to as the *inhomogeneity*, and $f \in L^2\left(\mathbb{R}^2\right)$ is a source term supported on K that depends on an incident wavefield. This problem can be reformulated into the Lippmann–Schwinger volume integral equation (LSE),

$$u^s(x) = \int_K \left[f\left(y\right) + k^2 m\left(y\right) u^s\left(y\right)\right] \Phi\left(x,y\right)\, dy, \qquad x \in \mathbb{R}^n, \tag{2}$$

where $\Phi(x,y)$ denotes the outgoing fundamental solution of the Helmholtz equation $\Delta u + k^2 u = 0$. In this talk, we discuss recent results provided in [1,2] concerning the development and practical implementation of provably accurate numerical methods to solve (2) in the case when ∂K is a self-similar fractal.

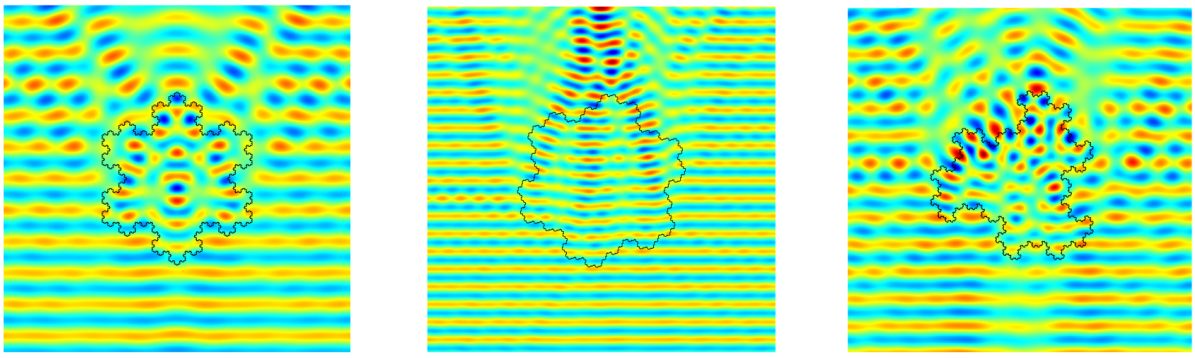

Figure 1: Scattering by the (Left) Koch snowflake, (Centre) Gosper Island and (Right) Fudgeflake for wavenumber $k = 30$. We have taken $1 + m = 1.311 + 2.289 \times 10^{-9} i$ for the Gosper Island and $1 + m = 2$ for the Koch snowflake and Fudgeflake.

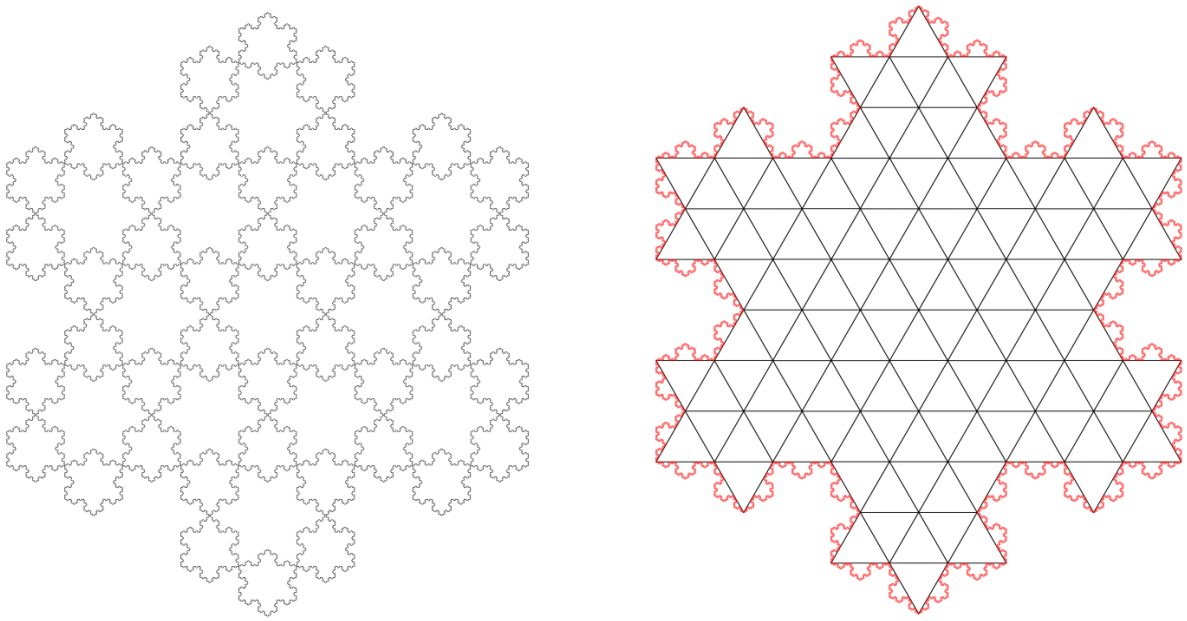

Figure 2: (Left) Self-similar geometry-conforming mesh of the Koch snowflake. (Right) A pre-fractal approximation equipped with a triangular mesh and full fractal boundary highlighted in red.

Method and results

We consider two distinct Galerkin-based approaches for (2) when ∂K is a self-similar fractal. For ease of presentation, we focus on the case when K is the Koch snowflake, a well-known fractal, as an illustrative example for both methods. The first class of methods, known as *pre-fractal methods*, rely on replacing the inhomogeneity K with a sequence of smoother (e.g., Lipschitz) sets, referred to as pre-fractals, that converge to K in a suitable sense, thereby permitting the use of conventional discretisation methods to solve the LSE. In contrast, the second class of methods require K to be an attractor of an iterated function system (IFS). Under standard technical assumptions on the IFS, K admits a sequence of quasi-uniform geometry-conforming meshes consisting of self-similar fractal elements, allowing the use of discontinuous piecewise polynomial approximation spaces to produce numerical approximations.

For both the IFS and pre-fractal method (for certain pre-fractals), we demonstrate that piecewise constant (PWC) Galerkin approximations of the LSE on suitable meshes are well-posed and converge asymptotically, satisfy the standard quasi-optimality bound and admit superconvergent estimates for the evaluation of linear functionals of the scattered field. For the IFS method, we show that the IFS approximation converges linearly to the solution of (2), and that evaluations of linear functionals, including evaluations of the scattered field away from K, converge quadratically, as one would expect for geometry-conforming PWC approximations. In contrast, the pre-fractal method converges at a significantly slower rate than the IFS method and depends on the Hausdorff dimension of ∂K, which we have validated numerically. Although the IFS method is decisively more accurate than the pre-fractal method, practically implementing the IFS method with PWC basis functions to approximate solutions of (2) requires confronting the following problems:

1. To assemble the resulting linear system, we must compute integrals of the form

$$\int_{K_i} f(x)\,dy \qquad \text{and} \qquad \int_{K_i}\int_{K_j} \Phi(x,y)\,dx\,dy, \tag{3}$$

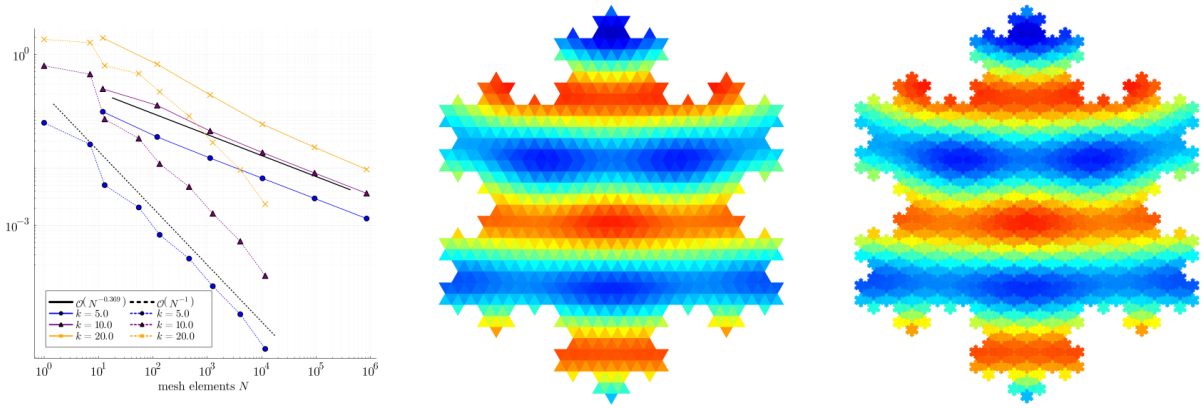

Figure 3: (Left) Error in scattered field for PWC IFS and pre-fractal approximations of the LSE. (Centre) Pre-fractal approximation of (2) with 128 triangular mesh elements. (Right) IFS approximation with 1261 self-similar mesh elements for $k = 15$ and $1 + m = 1.311 + 2.289 \times 10^{-9}i$.

where K_i and K_j denote scaled copies of the Koch snowflake which make up the self-similar mesh of the IFS method, f the source term of (1) and Φ is the fundamental solution of the Helmholtz equation. In other words, we must accurately approximate regular and weakly singular integrals over fractal sets to assemble the Galerkin equations.

2. Since LSE is a volume integral equation, the resulting linear system will be dense and typically larger than BEM matrices as the interior of K must be meshed as opposed to ∂K. Furthermore, the low-order nature of the method compounds these problems, rendering a naive implementation computationally infeasible.

Both problems are resolved by exploiting the mesh's self-similar geometry. Indeed, using recently developed quadrature methods for regular and weakly singular functions on IFS attractors [7,6], we can compute both types of integrals in (3) with rigorous error bounds. This allowed us to produce fully discrete error bounds for both the Galerkin approximation of the LSE and linear functional evaluations of the solution, ensuring that the predicted convergence rates are observed in practice. To resolve the second problem, we exploit the underlying lattice structures in the mesh geometry and the convolutional structure of the LSE to store the resulting linear system in linear complexity and to perform matrix-vector products in log-linear complexity using the fast Fourier transform. This dramatically reduces the storage costs of the linear system and the number of integrals that must be approximated via quadrature, and accelerates the use of iterative solvers, such as GMRES. Once again, our theoretical findings are validated by numerical results.

References

[1] J. Bannister, *Acoustic scattering by fractal inhomogeneities*, PhD thesis, UCL (University College London), 2024.

[2] J. Bannister, D. P. Hewett, and A. Gibbs, Acoustic scattering by fractal inhomogeneities via geometry-conforming galerkin methods for the lippmann-schwinger equation, *arXiv preprint* arXiv:2602.05005, 2026.

[3] A. J. Baran, A review of the light scattering properties of cirrus, *Journal of Quantitative Spectroscopy and Radiative Transfer*, 110 (2009), pp. 1239–1260.

[4] V. Coulibaly, D. Mikhailovskaia, and V. Nekoulin, Two methods of determination of ice crystal fractal dimension, *Scientific Prospects*, 9 (2012), pp. 5–7.

[5] D. L. Colton and R. Kress, *Inverse Acoustic and Electromagnetic Scattering Theory*, Springer, 4th edition, 2019.

[6] A. Gibbs, D. P. Hewett, and B. Makarov, Numerical evaluation of singular integrals on non-disjoint self-similar fractal sets, *Numerical Algorithms*, 97 (2024), pp. 311–343.

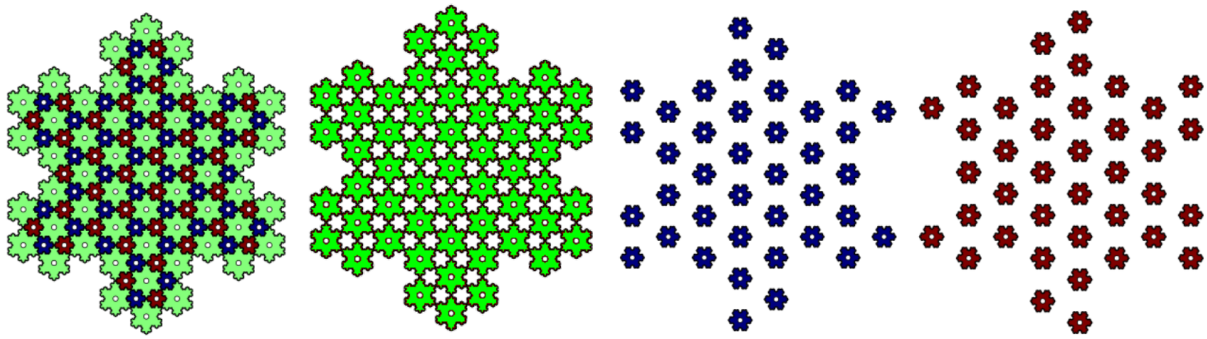

Figure 4: A self-similar mesh of the Koch snowflake decomposed into three collections of identical mesh elements with an identical lattice structure.

[7] A. Gibbs, D. Hewett, and A. Moiola, Numerical quadrature for singular integrals on fractals, *Numerical Algorithms*, 92 (2023), pp. 2071–2124.
[8] A. Moiola and E. A. Spence, Acoustic transmission problems: wavenumber-explicit bounds and resonance-free regions, *Mathematical Models and Methods in Applied Sciences*, 29 (2019), pp. 317–354.
[9] T. H. Stein, C. D. Westbrook, and J. Nicol, Fractal geometry of aggregate snowflakes revealed by triple-wavelength radar measurements, *Geophysical Research Letters*, 42 (2015), pp. 176–183.
[10] J. Tufenkji, J. Leinonen, D. Moisseev, and T. Nousiainen, Radar backscattering from snowflakes: Comparison of fractal, aggregate, and soft spheroid models, *Journal of Atmospheric and Oceanic Technology*, 28 (2011), pp. 1365–1372.

* * *

Numerical Solution of Time Fractional Black–Scholes Equation using Radial Basis Functions and Chebyshev Polynomial Collocation Method

H. Bansu, S. Margenov

The valuation of financial derivatives, particularly options, has been a central topic in quantitative finance since the introduction of the classical Black–Scholes (B–S) model in 1973. This model provides a mathematical framework for pricing European options under idealized assumptions such as constant volatility and frictionless markets. Despite its widespread success, the classical B–S model fails to capture several empirical features of financial markets, including memory effects, long-range dependence, and anomalous diffusion. To address these limitations, fractional calculus has been introduced into financial modeling, leading to the development of the time-fractional Black–Scholes (TFBS) equation, which incorporates nonlocal temporal dynamics through fractional derivatives.

In this study, we consider a time-fractional Black–Scholes model formulated using the Caputo fractional derivative of order $0 < \alpha \leq 1$. The inclusion of fractional derivatives enables the model to account for memory and hereditary properties of financial markets, thereby providing a more realistic description of asset price dynamics. However, the resulting fractional partial differential equation is analytically intractable in most cases, necessitating the use of efficient and accurate numerical techniques.

To overcome this challenge, we propose a hybrid collocation method that combines radial basis functions (RBFs) for spatial discretization with Chebyshev polynomials for temporal approximation. The method is constructed by first transforming the original TFBS equation using a logarithmic change

of variables, which converts the unbounded spatial domain into a more convenient form. The problem is then restricted to a finite computational domain to facilitate numerical implementation.

In the proposed framework, the unknown solution is approximated as a linear combination of RBFs in space and Chebyshev polynomials in time. The use of RBFs provides a mesh-free approximation, which is particularly advantageous for handling irregular domains and avoiding grid generation complexities. In this work, cubic radial basis functions (polyharmonic splines) are employed due to their simplicity and good approximation properties. On the other hand, Chebyshev polynomials are utilized for temporal discretization because of their spectral accuracy and rapid convergence.

The governing TFBS equation is enforced at selected collocation points in both space and time, leading to a system of algebraic equations. By applying the collocation procedure along with the given boundary and initial conditions, the problem is reduced to a linear system expressed in matrix form using Kronecker products. This formulation allows for efficient computation of the unknown coefficients and facilitates straightforward implementation using standard numerical solvers.

To validate the effectiveness of the proposed approach, numerical experiments are performed.It is observed that the hybrid RBF–Chebyshev collocation method achieves high accuracy, fast convergence and computational efficiency. Additionally, the method demonstrates flexibility in handling fractional orders and can be easily extended to other types of fractional differential equations.

In conclusion, the proposed hybrid collocation scheme provides a powerful and efficient numerical tool for solving the time-fractional Black–Scholes equation. Its mesh-free nature, makes it particularly suitable for complex financial models involving fractional dynamics. The approach not only improves the accuracy of option pricing but also opens new avenues for the application of fractional calculus in financial engineering.

* * *

Bias Correction of EURO-CORDEX High-Resolution Simulations: Evaluation on the Near Past Climate over Southeast Europe

H. Chervenkov, K. Slavov

Regional climate models (RCMs) have been widely used to downscale coarser general circulation model (GCM) simulations and to provide fine-scale regional climate information, supporting more detailed impact and adaptation assessment and planning. The RCMs' output, however, may exhibit large biases, inherited from the driving GCM, in addition to those introduced by the RCMs. Persistent biases can undermine the reliability of climate projections, making it difficult for policymakers and stakeholders to make effective adaptation plans. Various methods have been created to minimize and correct these biases as sources of error in subsequent modelling chains. Our study evaluates the performance of the distribution-wise bias correction (BC) or adjustment method, quantile delta mapping (QDM), applied to 14 EURO-CORDEX GCM/RCM combinations, employing a consistent framework to compare its productivity and effectiveness with the ERA5-Land reference in the period 1976 to 2005. The examined variables are the daily minimum, mean, and maximum temperatures, as well as the precipitation sum. To address both long-term (e.g., decadal) natural climate variability and intermodel variability, a relatively extended calibration period and a large number of model runs are utilized within a more rigorous evaluation framework that separates calibration and evaluation periods. Specifically, the years 1951 to 1975 are used for calibration, and 1976 to 2005 are reserved for evaluation, ensuring a transparent division between the two phases. In aggregating results, each model is assigned equal weight. Emphasis on median-based (X50) estimates aligns with standard practice in the field, providing robustness against

outliers and reducing the risk of overfitting to individual model characteristics. Additionally, to estimate the intermodel spread, we compute the lower and upper quartiles (X25&X75) of the multimodel ensemble (MME). To explicitly address intra-annual variations and the impact of the QDM on derived parameters, the evaluation is performed using monthly means and sums, as well as key climate indices of the Expert Team on Climate Change Detection and Indices (ETCCDI). Specifically, we consider the threshold indices frost and summer days, the duration index consecutive dry days, and the percentile index precipitation in very wet days. Given the large amount of involved data and the extensive processing required, the study can be regarded as both a big data and a large-scale scientific computation task. To facilitate this, we design a special workflow embedded in the purpose-build routine, as shown in Figure 1. It is widely recognized that bias adjustment methods can significantly affect the mean values of climate time series, and our results confirm this common conclusion. Most generally, the outcomes show that the BC output is highly variable, magnitude-, quantile-, and region-dependent. Overall, we provide strong evidence that QDM performs very well across most of the domain, significantly minimizing biases in the raw GCM/RCM output in all months. Consistent with previous findings, we show that QDM reduces the biases in daily minimum, mean (Figure 2), and maximum temperatures by up to one order of magnitude. The degree of reduction in the precipitation bias is smaller but still significant. Furthermore, QDM significantly affects nonlinearly derived indicators of extremes, such as the investigated threshold climate indices. The index consecutive dry days is moderately affected, and the index precipitation in very wet days appears as the most error-prone. Regardless of the results, which are judged as very promising, care must be taken when carrying out the bias adjustment process.

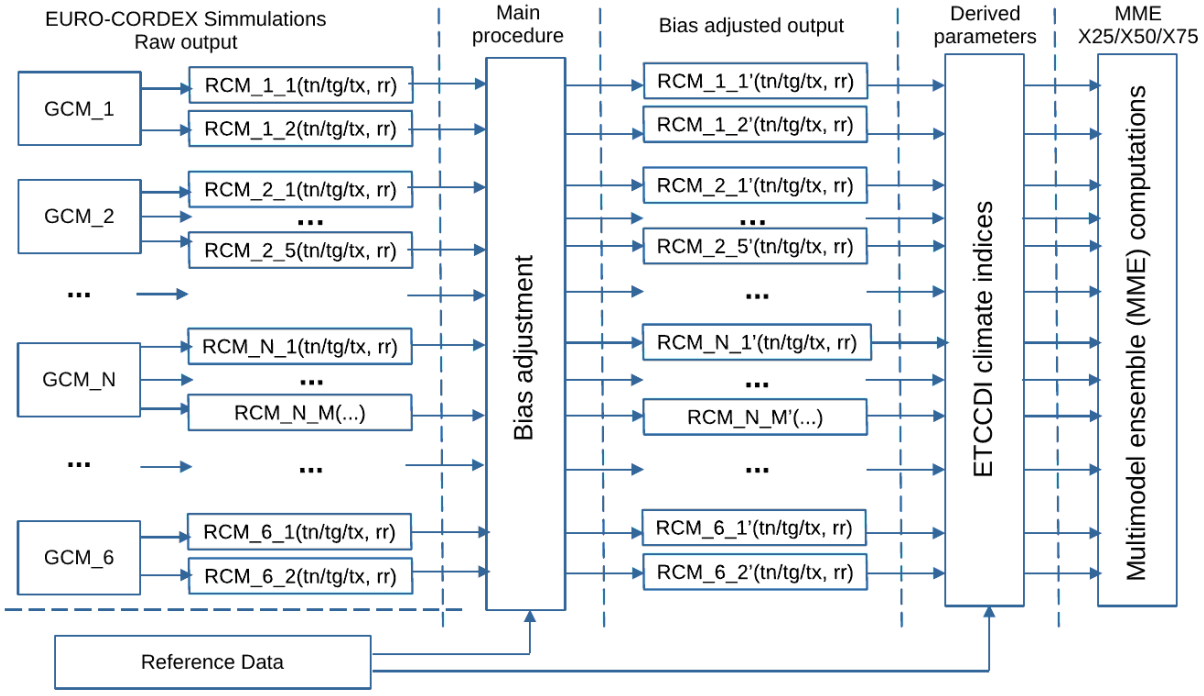

Figure 1: Data workflow in the computational routine

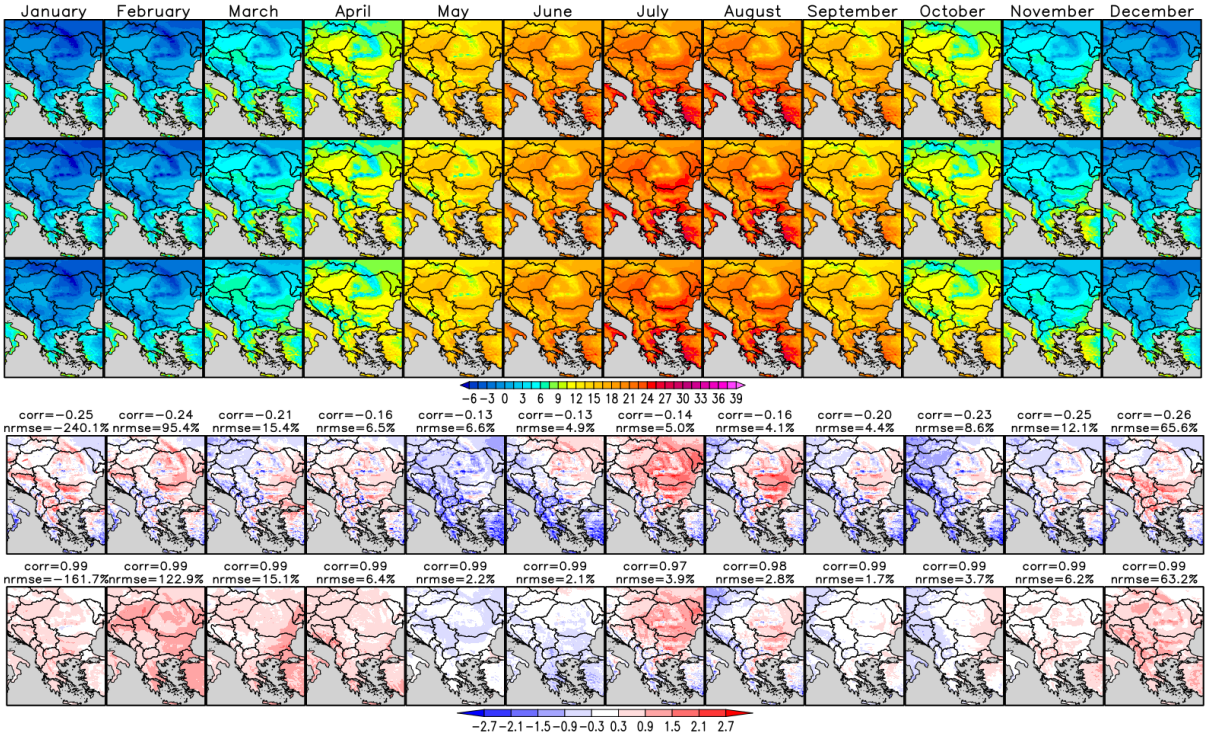

Figure 2: Multiyear mean values for 1976–2005 of the mean monthly temperature (unit: °C) of the reference, MME X50 of the uncorrected and MME X50 of the corrected GCM/RCM output on the first, second and third row correspondingly. The absolute bias of the uncorrected and the corrected output are shown on the fourth and fifth row correspondingly. The field means of the corr and NRMSE are reported over each bias subplot.

* * *

Numerical Modeling Strategies for Intrinsically Disordered Protein Aggregation Mechanisms

M. Chwastyk

Intrinsically disordered proteins (IDPs) play a central role in a wide range of aggregation-driven biological processes, yet their structural heterogeneity poses significant challenges for conventional modeling approaches. In this talk, I will present a computational framework designed to investigate the early stages and progression of IDP aggregation at the molecular level. Our strategy combines coarse-grained and all-atom representations to efficiently capture both large-scale assembly behavior and detailed interaction patterns. Initial conformational ensembles are generated to reflect the intrinsic flexibility of disordered regions, followed by molecular dynamics simulations in explicit solvent to probe aggregation pathways and transient intermolecular contacts. To quantify aggregation propensity and structural features, we employ trajectory-based analyses, including contact persistence, cluster formation metrics, and conformational diversity assessment. This integrative approach enables the identification of key determinants governing aggregation mechanisms and provides insight into the dynamic interplay between disorder, interaction specificity, and self-assembly. The proposed methodology offers a generalizable approach for studying aggregation phenomena in disordered protein systems.

* * *

Extending Quantum Annealing to Continuous Optimization

H. Djidjev

Quantum annealing is a promising approach for solving difficult discrete optimization problems, especially problems that can be written in Ising or QUBO form. Current quantum annealing hardware, however, is naturally designed for binary variables, while many important optimization problems in computer science, engineering, finance, logistics, and scientific computing involve continuous decision variables. A common way to bridge this gap is to discretize each continuous variable into several binary variables, but this can greatly increase problem size, introduce numerical scaling issues, and limit the size of problems that can be handled on present-day hardware.

This talk presents **Quantum Enhanced Simulated Annealing (QESA)**, a hybrid quantum-classical framework for applying quantum annealing to continuous optimization without fully discretizing the original variables. The main idea is simple: instead of asking the quantum annealer to solve the entire continuous problem, we use it to choose promising search directions inside a classical simulated annealing loop. At each iteration, the current continuous solution is updated by moving in a direction selected from a large discrete set. That direction-selection subproblem can be written as an Ising model, making it suitable for quantum annealing. The resulting candidate point is then projected back into the feasible continuous domain, and a simulated annealing acceptance rule determines whether the move is accepted.

We demonstrate this approach on box-constrained quadratic programming, a fundamental continuous optimization problem that becomes challenging when the quadratic objective is nonconvex. This setting provides a useful test case because it is simple to state, practically relevant, and closely connected to both continuous optimization and binary Ising formulations.

Experimental results on randomly generated quadratic programs show that QESA can produce high-quality solutions across a range of problem sizes and conditioning regimes. In the reported experiments, it consistently improves over standard simulated annealing and several classical heuristic baselines, and in some time-limited cases matches or improves upon the solution quality obtained by a state-of-the-art commercial solver. More broadly, the talk illustrates how near-term quantum annealers can be used not as standalone solvers for entire continuous problems, but as specialized components inside larger classical optimization algorithms.

Acknowledgements

This work was partially supported by the Centre of Excellence in Informatics and ICT under Grant No.BG16RFPR002-1.014-0018-C01, financed by the Research, Innovation, and Digitalization for Smart Trans formation Programme 2021-2027 and co-financed by the European Union.

* * *

Multilevel Methods for Optimal Control of Elliptic Equations with Stochastic Coefficients Discretized Using Stochastic Collocation

A. Draganescu, B. Sousedik, S. Alzuhairy

The aim of this research is to develop efficient multigrid preconditioners for a classic linear-quadratic optimization problem constrained by an elliptic equation with stochastic coefficients. Using a discretize-then-optimize approach, we have shown that strategies inherited from the associated deterministic optimal control problem extend to the stochastic version when using either a stochastic Galerkin or a sparse grid stochastic collocation discretization.

* * *

Medical Sorting of Earthquake Victims

S. Fidanova, N. Bozakova, V. Ivanov

1 Introduction

Natural disasters can cause not only major material damage, but also a large number of casualties. An important element of the organization of rescue activities is medical sorting. This study concerns medical sorting and assistance to earthquake victims. The sorting stages will be primary assessor of whether the injured person will survive, pre-hospital and in-hospital. Cluster analysis will be applied at each sorting stage. The goal is to provide rapid medical care to the injured and reduce the number of fatalities.

2 Medical Triage

Medical triage is a method of distributing victims into groups depending on the need for uniform treatment, prevention and evacuation measures in connection with medical indications. It is of particular importance in disaster situations. Medical triage determines the priorities in terms of medical care. Not all victims can immediately receive the necessary assistance, which is why some selection of victims is simply inevitable.

3 Triage Algorithm

In this study, we propose several stages of triage. Clister analysis will be used to triage the victims. The triage stages are as follows:

- First stage triage: who are likely to live;
- Second stage triage: hospital or ambulatory;
- Third stage: who needs immediate care.

Grouping large groups of objects according to their similarity is called cluster analysis. There are two main types of cluster analysis: hierarchical clustering and K-means clustering.

The clustering is hierarchical when the number of clusters and their centroids are not known in advance.

In K-means clustering the number of clusters is known and we can define the centroid of each one. There is a set of characteristics that the objects of the cluster correspond to,and a function that shows the distance of a given object to the centroid.

The first triage stage is based on the chances of survival. It is performed at the event location. In this case, there are two clusters: with a chance of survival, and no chance of survival.

Another triage, which is performed on the place of event location is regarding the need for hospitalization. It corresponds to the severity of the injury.

The third triage is done in a hospital. There they are sorted according to the type of injury and its severity. The most severe injury is treated first.

4 Conclusion

Earthquakes cause a large number of casualties. Some have no chance of survival. Those who have a chance of survival may have injuries of varying types and severity. They must be classified. With the proposed model, we aim to improve the organization of providing assistance to earthquake victims.

Acknowledgements

The work is supported by National Scientific Fund of Bulgaria under the grant DFNI KP-06-N82/2. The work was partially supported by the Centre of Excellence in Informatics and ICT under the Grant No BG16RFPR002-1.014-0018-C01, financed by the Research, Innovation and Digitalization for Smart Transformation Programme 2021-2027 and co-financed by the European Union.

* * *

The Condition of a Cow Farm After an Earthquake

S. Fidanova, N. Bozakova, M. Shopov, V. Ivanov

1 Introduction

Natural disasters cause severe damage to ordinary people and the economy of the region in which they occur. If there is a farm in the area, this can lead to additional complications. Animals panic more easily than humans during an earthquake, which can lead to additional damage, disruption of food supplies, contamination of water sources, and epidemics. Mathematical models are used to minimize negative consequences. With their help, preliminary assessments of the consequences can be made and measures can be taken to prevent them. In this paper, we focus on assessing the consequences of an earthquake on a dairy farm. We take into account the number of animals injured and the severity of their injuries, the number of animals killed, and the risk of an epidemic.

2 Mathematical Model of Cow Farm and Earthquake

Humans feel earthquakes with a magnitude greater than 3, while animals are more sensitive and can feel even weaker earthquakes. This can lead to anxiety and even panic in them. When we have a weak to

medium earthquake, with a magnitude between 5 and 7, there may be damage to less resistant buildings. In this case, the level of anxiety and panic in animals is at a lower level and, accordingly, the resulting damage is smaller. In this case, the number of injured and dead animals as a result of panic is small and the probability of an epidemic due to contamination is low. In stronger earthquakes, with a magnitude of between 7 and 8, the level of panic among animals increases and this can lead to a greater number of injured and dead animals. In this case, there is a greater likelihood of an epidemic occurring. In strong earthquakes, with a magnitude of more than 8, panic among animals is great. This leads to crowds and collisions between them and, accordingly, to a large number of injured and dead animals. In this case, the probability of an epidemic is very high. In this study we estimate the injured cows, those with serious injuries and needing to be euthanized, as well as the dead animals as a percentage of all animals in the farm. On the basis of number of dead animals we estimate the danger of epidemic. The estimates made in this way are approximate, but realistic enough to be used for preliminary preparation.

The software implementation of the model is made in the programming language C. The evaluation parameters are input data. Thus, they can be easily changed according to the judgment of the specialists. The input data of the model are as follows: earthquake intensity; number of animals; building resistance.

3 Conclusion

Farms are being consolidated and farms for several thousand animals are being created with the automation of some of the processes involved in raising them. created with the automation of some of the processes involved in raising them. This increases the quality of cultivation and reduces the cost of production. When such a farm is located in an earthquake zone, it can create additional problems. As a result of panic and animal collisions, there may be deaths of animals, leading to the risk of contamination of water sources and epidemics. In this paper, we propose a methodology for assessing the number of injured and dead animals, and hence the risk of an epidemic, as a function of the total number of animals and the strength of the earthquake.

Acknowledgement
The work is supported by National Scientific Fund of Bulgaria under the grant DFNI KP-06-N82/2. The work was partially supported by the Centre of Excellence in Informatics and ICT under the Grant No BG16RFPR002-1.014-0018-C01, financed by the Research, Innovation and Digitalization for Smart Transformation Programme 2021-2027 and co-financed by the European Union.

* * *

Informed Strategy for Targeted Therapeutics Design

N. Ilieva, P. Petkov, E. Lilkova, and L. Litov

Viruses rely on a small set of proteins to invade and hijack host cells — but these same proteins can also reveal how to stop infection. In this talk, I will discuss how computer modeling and artificial intelligence can uncover the structure and dynamics of key coronavirus proteins, highlighting their most vulnerable sites. By combining molecular dynamics simulations with a novel AI-based technique — a convolutional neural network (CNN) trained to estimate the binding free energy of protein–protein complexes — we aim to transform viral proteins from agents of infection into blueprints for new antiviral therapeutics.

Our attention is directed toward peptide aptamers — short combinatorial sequences of 5–20 amino acids capable of specifically binding diverse target molecules. This makes them a powerful tool for modulating or inhibiting biological functions and places them in the fastest-growing class of therapeutics: protein-based bioactive agents.

We explore how small, exceptionally stable natural peptides, known as cyclotides, can be employed in blocking viral targets. Cyclotides, mini-proteins with a head-to-tail cyclized backbone and a cystine knot motif (CKM) composed of three interlocking disulfide bonds, serve as exceptional scaffolds for peptide aptamers. By embedding aptamer sequences into one of the cyclotide's loop regions — a process known as grafting — modified molecules can be created that retain the cyclotide's extraordinary structural stability while gaining targeted binding functionality.

Thet study centers on two peptides of our original discovery: one targeting the accessory protein ORF6, and a second targeting the helicase NSP13 of the SARS-CoV-2 virus. To translate these active peptides into potential drug candidates, they are strategically grafted onto cyclotide scaffolds, combining their inhibitory function with the exceptional stability of the cyclotide framework. Next to all-atom MD simulations, coarse-grained simulations are employed to accelerate variant screening, enabling rapid evaluation of multiple molecular designs.

This pilot study opens new perspectives for the development of biological agents with potential therapeutic applications and practical impact in medicine and pharmaceutics.

Acknowledgements
This research was partially funded by the Bulgarian National Science Fund under Grants KP-06-N71/3/2023 AVATAR and KP-06-COST-20/2023 INSISTT. We acknowledge stimulating discussions within the COST Action CA21169 "Information, Coding, and Biological Function: The Dynamics of Life (DYNALIFE)".

Computational resources were provided at the Discoverer supercomputer – Sofia (Bulgaria), thanks to Discoverer PetaSC and EuroHPC JU, by the HPC cluster BioSim at the Physics Faculty of the Sofia University "St. Kl. Ohridski" (Bulgaria), and at the Tricity Academic Supercomputer & networK Centre (CI TASK) – Gdansk (Poland).

* * *

Predicting Eathquaqe Using Cows as a Biosensors

S. Fidanova, V. Ivanov, N. Bozakova

1 Introduction

Earthquakes cause enormous material damage and human casualties. Even a few hours' warning would have saved many lives. Some animals are much more sensitive than human to changes in the vibrations and ionization of the earth's crust. In this work, we propose the use of cows as biosensors for short-term earthquake prediction. We have proposed an algorithm for monitoring changes in cow behavior and from there assessing the possibility of an earthquake occurring.

2 Algorithm for Earthquake Prediction

The main idea of current study is to use cows as biosensors for early prediction of an approaching earthquake.

We will use the following changes in cow behavior:

- Decrease in milk supply. Appears up to 3 weeks before the earthquake;
- Descending from the mountain into the lowlands. Appears 4 days before the earthquake;
- Refusal to enter a confined space (stall), Appears 4 days before the earthquake;
- Increased activity, From 1 to 20 hours before the earthquake;
- Loud moaning, displays of aggression. Just before the earthquake.

Such an algorithm for monitoring and tracking changes in cow behavior in a given earthquake area allows for early preparation of authorities and the population and for an adequate response.

3 Conclusion

Cows are very sensitive to changes preceding earthquakes. We have proposed an algorithm for monitoring changes in cow behavior to predict an approaching earthquake. This way, people will be able to leave the buildings they are in and go to a safe place. Such algorithms are cheap to implement, and could save many lives.

Acknowledgements
The work is supported by National Scientific Fund of Bulgaria under the grant DFNI KP-06-N82/2 and by the Polish-Bulgarian collaborative grant "Practical aspects for scientific computing". The work was partially supported by the Centre of Excellence in Informatics and ICT under the Grant No BG16RFPR002-1.014-0018-C01, financed by the Research, Innovation and Digitalization for Smart Transformation Programme 2021-2027 and co-financed by the European Union.

* * *

Exploring Maximum Principles in Fractional Diffusion-Reaction Equations

S. Harizanov, S. Margenov

The maximum principle is a fundamental property of elliptic boundary value problems, ensuring that the solution attains its extrema on the boundary. Preserving this property at the discrete level is essential for the stability and reliability of numerical simulations. In this work, we investigate multidimensional fractional diffusion-reaction problems, focusing on spectral fractional operators, which pose new challenges due to their nonlocal nature.

Discretization is carried out using both finite difference and finite element methods, with lumped mass matrices applied in the latter to maintain stability. A major computational challenge arises from the dense linear systems generated by fractional operators, particularly in large-scale multidimensional settings in domains of general shape. To address this, we employ Best Uniform Rational Approximation (BURA) techniques, which allow for efficient and scalable solution of these systems.

Beyond computational efficiency, we study qualitative properties of the numerical solutions. Specifically, we analyze conditions under which discrete maximum principles hold for the chosen discretization methods, as well as conditions ensuring monotonicity of BURA-based approximations. Our contributions are threefold: (i) derivation of maximum principles for fractional diffusion-reaction problems;

(ii) sufficient conditions for discrete maximum principles in the numerical schemes; and (iii) sufficient conditions for monotonicity in BURA and BURA-like approximations.

The theoretical analysis focuses on subdiffusion with fractional power $\alpha \in (1/2, 1)$ and constant reaction coefficients, providing rigorous criteria for both stability and monotonicity. These findings are further illustrated and validated through a set of representative numerical experiments, demonstrating the practical applicability of the proposed methods in multidimensional simulations. The results highlight the interplay between discrete maximum principles, monotonicity, and computational efficiency in the numerical treatment of fractional diffusion-reaction problems.

For further details, see [1].

Acknowledgements

This work was partially supported by the Centre of Excellence in Informatics and ICT under Grant No.BG16RFPR002-1.014-0018-C01, financed by the Research, Innovation, and Digitalization for Smart Trans formation Programme 2021-2027 and co-financed by the European Union, and by the Bulgarian National Science Fund under Grant No.KP-06-N72/2.

References

[1] Harizanov, S.; Margenov, S. Maximum Principles for Fractional Diffusion Problems. *Symmetry* **2026**, *18*, 272.

* * *

Error Balancing when Solving Fractional Elliptic Equations

S. Harizanov, D. Slavchev, N. Kosturski

We consider fractional elliptic equations $\mathcal{A}^\alpha u = f$, where the fractional power α is larger than one. They are related to super-diffusion. After a finite difference (FD) discretization such equations are in the form:

$$\mathbb{A}^\alpha \mathbf{u} = \mathbf{f}, \quad \alpha > 1.$$

Even though $\mathbb{A}$ is a sparse SPD matrix with a nice structure, its α-th power is everywhere dense, thus for large scale real-life problems it is impractical (and sometimes even impossible) to compute the exact solution. Therefore, we apply the product BURA method, introduced in [1], to derive an approximate solution for it. The theoretical approximation error of the method is

$$E_{\bar{\alpha}} = 1 - \prod_{i=1}^{\ell} (1 - E_{\alpha_i}), \qquad \alpha = \sum_{i=1}^{\ell} \alpha_i, \quad \alpha_i \in (0, 1],$$

where E_{α_i} are the corresponding approximation errors for the classical BURA method with $\alpha_i \in (0, 1]$. Here, the error function is not equi oscillating, but consists of increasing oscillations in the unit interval. Applying the standard λ_1-normalization to the BURA solver, where λ_1 is the smallest eigenvalue of $\mathbb{A}$, we allow for the approximation error to reach its maxima for $\mathbf{f} = \mathbf{f}_1$, $\mathbf{f}_1$ being the eigenvector of $\mathbb{A}$ that corresponds to λ_1. In this talk, we propose a different normalization, namely the $\varepsilon_{2k+1}^{-1}\lambda_1$ one, where ε_{2k+1} is the largest zero of the error function and (k, k) is the order of the corresponding α_i BURA element.

In this setup, the approximation error for $\mathbf{f} = \mathbf{f}_1$ is zero, and the derived error estimates are significantly smaller. Furthermore, the ratio between the theoretical estimate $E_{\bar{\alpha}}$ and the concrete error for a given right-hand-side f depends mainly on the spectral decomposition of f over $\mathcal{A}$ and behaves quite

stably with respect to changing the discretization step in FD. This allows us to choose a proper order k, smaller than the theoretically proposed one, in order to balance the FD discretization error and the product BURA approximation error.

Acknowledgements
This work was partially supported by the Centre of Excellence in Informatics and ICT under Grant No.BG16RFPR002-1.014-0018-C01, financed by the Research, Innovation, and Digitalization for Smart Trans formation Programme 2021-2027 and co-financed by the European Union, and by the Bulgarian National Science Fund under Grant No.KP-06-N72/2.

References
[1] Slavchev, D., Harizanov, S., Kosturski, N. Analysis on computational issues when approximating fractional powers of sparse SPD matrices. *International Journal of Applied Mathematics* **2024**, *37(6)*, pp. 699-711.

* * *

Investigation of the Relationship Between Rumination Activity and Eye Temperature in Dairy Cows Under Mild Heat Stress Using Infrared Thermography

H. Hristov, K. Dimitrov, T. Penev

Abstract

This extended abstract examines whether infrared thermography of the eye can provide useful information about physiological and behavioural responses of dairy cows exposed to mild heat stress. Measurements were obtained under field conditions in Bulgaria from eleven dairy cows. For each observation, the temperature–humidity index (THI) was recorded, an infrared image of the eye region was acquired, and rumination activity was noted. Minimum, average, and maximum eye temperatures were extracted from the thermograms. Because the sample was small, the statistical analysis was intentionally compact and transparent. Descriptive statistics and the Shapiro–Wilk test were used for initial characterization of the data, while the main associations were examined with targeted Spearman rank correlations. The results showed clear positive relationships between THI and both average and maximum eye temperature, indicating that infrared eye thermography is sensitive to environmental heat load even within a relatively narrow range of mild stress. The relationship between THI and rumination activity was weaker and did not reach the conventional level of statistical significance. A significant positive correlation was also observed between maximum eye temperature and rumination activity, but this result should be interpreted cautiously because of the exploratory character of the study and the limited number of animals. Overall, the findings support the potential of infrared eye thermography as a practical non-contact tool for monitoring heat-related response in dairy cows.

1 Introduction

Heat stress is an important factor affecting dairy cow welfare, behaviour, and productivity. Its relevance is not limited to periods of severe thermal challenge, because even moderate environmental load may disturb thermoregulation and alter behavioural indicators such as feeding or rumination. For this reason,

non-contact methods capable of detecting early heat-related changes are of practical interest in dairy production.

Infrared thermography is attractive because it is rapid, non-invasive, and suitable for field conditions. The eye region is commonly regarded as a promising target, since it is physiologically responsive and comparatively easy to image. Rumination activity, in turn, is a useful behavioural indicator linked to digestive function and general comfort. The present work explores whether simple relationships can be identified among THI, infrared eye temperature, and rumination activity in dairy cows exposed to mild heat stress.

2 Materials and Methods

The observations were carried out under farm conditions in the region of Stara Zagora, Bulgaria. Eleven dairy cows were included in the present dataset. For each animal, THI was recorded close to the cow using a Kestrel 5400 instrument. Infrared images of the eye region were then acquired with a FLIR E6 thermal camera under comparable observational conditions.

From each thermogram, three descriptors were extracted: minimum eye temperature, average eye temperature, and maximum eye temperature. Rumination activity was recorded for each animal and treated as the behavioural variable of interest. Thus, each row in the dataset contained one THI value, three eye-temperature measures, and one rumination count. Given the limited sample size, the study emphasized interpretability and restraint rather than complex modelling.

3 Statistical Approach

The analysis began with descriptive statistics for all variables, including the mean, standard deviation, median, quartiles, interquartile range, minimum, and maximum. The Shapiro–Wilk test was then applied as a preliminary check of distributional shape. Because the sample was small and the behavioural variable showed borderline distributional behaviour, the main associations were evaluated using Spearman rank correlation.

The targeted pairs were THI with average eye temperature, THI with maximum eye temperature, THI with rumination activity, and maximum eye temperature with rumination activity. In addition, scatter plots were prepared for THI versus average eye temperature and THI versus maximum eye temperature to provide a visual representation of the two principal temperature-related relationships.

4 Results and Discussion

The descriptive statistics indicate a relatively narrow but meaningful range of mild heat stress conditions. The mean THI was 74.45 with a standard deviation of 1.91, and the observed values ranged from 72.1 to 79.0. The thermographic variables showed limited dispersion: the mean minimum eye temperature was 35.54 °C, the mean average eye temperature was 36.05 °C, and the mean maximum eye temperature was 36.36 °C. Their standard deviations were below 0.50 °C. By comparison, rumination activity varied more widely, with a mean of 483.18, a standard deviation of 68.30, and a range from 352 to 591. This difference suggests that behavioural response may depend on factors beyond the thermal variables measured here.

The Shapiro–Wilk test did not indicate a clear departure from normality for THI or for the thermographic variables. Rumination activity produced a borderline result, which supported the use of a nonparametric association method. Spearman analysis revealed a strong positive association between THI and average eye temperature ($\rho = 0.751710$, $p = 0.007634$), as well as between THI and maximum

eye temperature ($\rho = 0.736364$, $p = 0.009760$). These findings indicate that increasing environmental heat load was accompanied by increasing infrared eye temperature, even within the restricted range of mild heat stress represented in the dataset.

The relationship between THI and rumination activity was weaker ($\rho = 0.566216$, $p = 0.069388$) and did not reach the conventional significance threshold. This result suggests a tendency, but not sufficiently strong statistical support for a firm conclusion. A significant positive association was found between maximum eye temperature and rumination activity ($\rho = 0.748866$, $p = 0.008000$). Although this result is noteworthy, it should be interpreted carefully. The sample is small, the conditions correspond to mild rather than severe heat stress, and rumination is influenced by multiple additional factors such as feeding schedule, individual physiology, and management context.

The scatter plots for THI versus average eye temperature and THI versus maximum eye temperature visually support the numerical results, showing a clear upward trend rather than a random cloud of points. This agreement between visual and statistical evidence strengthens the conclusion that infrared eye thermography captures heat-related variation in the examined animals. At the same time, the behavioural findings are best regarded as exploratory and hypothesis-generating.

5 Conclusions

The present extended abstract provides a compact analysis of THI, infrared eye temperature, and rumination activity in dairy cows under mild heat stress. The principal result is that THI showed strong positive associations with both average and maximum eye temperature, supporting the use of infrared eye thermography as a promising non-contact indicator of heat-related physiological response.

The associations involving rumination activity were less robust. Although maximum eye temperature correlated positively with rumination count, the relationship between THI and rumination activity remained below the conventional significance threshold. Therefore, the rumination-related findings should be treated as exploratory. Overall, the study demonstrates that a small field dataset can still provide meaningful evidence when the statistical approach remains clear and restrained. Future work should include larger cohorts, repeated measurements, and broader environmental ranges in order to evaluate the combined diagnostic value of thermographic and behavioural indicators more rigorously.

* * *

Recurrence of Cold and Frosty Conditions in RCP2.6, RCP8.5 Scenarios and Historical Climate over Bulgaria

V. Ivanov, I. Georgieva, G. Gadzhev

Abstract

The future climate changes show increasing and even decreasing of the mean temperature depending on the continent and the corresponding region. The projections show the Mediterranean as one of the future hot spots, and Bulgaria as a part of Balkan region, has a similar climate conditions. That lead to the question how that change would affect the human thermal in the future. The current research is trying to give an answer if the climate changes influence on the cold feeling over the territory of Bulgaria. The results suggest that the distribution of the UTCI cold categories shows a spatial and diurnal diversity

most pronounced at early morning and in midnight hours for both of the scenarios. That would be of interest for the tourist industry, mainly for the winter segment in Bulgaria.

1 Introduction

The motivation for the current research is the need for envision of how the future climate changes influence on the cold feeling over the territory of Bulgaria. That study would it be of interest for the tourist industry, mainly for the winter segment in Bulgaria. In that way, not only the tour-agents, and the hoteliers, but also the Mountain Rescue Service could plan their future investments in a more reliable manner. The aim of the current research is to investigate the change of the cold and freezing conditions recurrences for two future emission scenarios – optimistic (RCP2.6) and pessimistic (RCP8.5) over Bulgaria.

2 Methods

The data from the global climate models are with coarser resolution, which does not takes into account the finer topography of given domain. That imposes an applying of dynamical downscale technique with initial and boundary conditions from the former models to regional ones. In the current study, we use the outputs from the Global Earth-System Model HadGEM2-ES and the regional climate model RegCM4 is configured according to the spatial features of the domain under consideration [1,2]. The model simulations cover the periods from 01.01.1975 to 31.12.2004 (historical scenario), and from 01.12.2069 to 30.11.2099 (future scenarios).

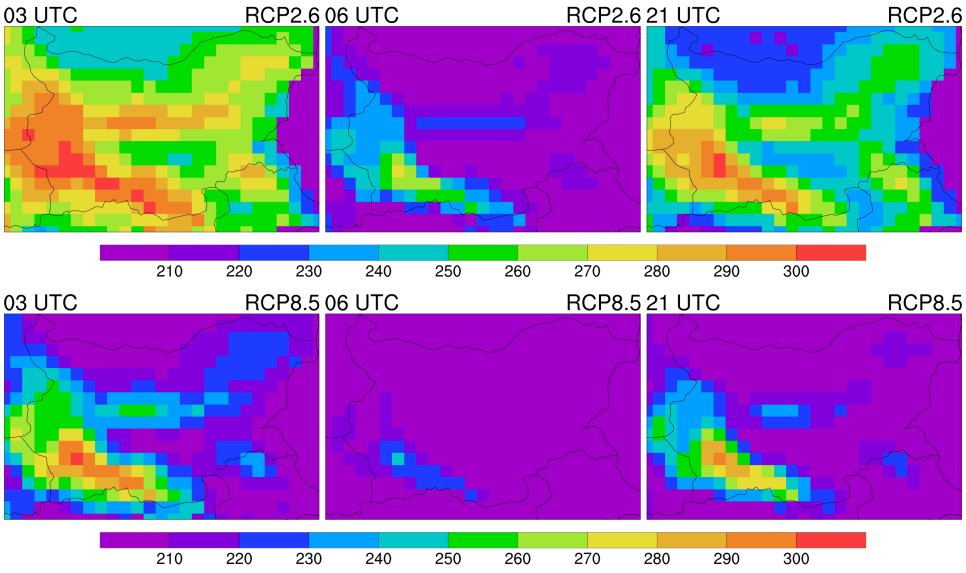

Figure 1: Yearly-average number of cases with ”cold” UTCI categories for the optimistic scenario (RCP2.6) and pessimistic scenario (RCP8.5).

The estimation of the climate change is performed on the base of the historical climate and future emission scenarios. The current work estimates the influence of the optimistic (RCP2.6) which suggests that the emissions do not undergo a strong reduction, and the pessimistic (RCP8.5), where the countries do not take regulatory measures for emissions reduction in their future economic development [3,4]. For estimating of the influence of the cold and freezing conditions on the human beings, the Universal

Thermal Climate Index (UTCI) is calculated [5], used in many previous studies [6,7]. At the present study are shown simulations for these three hours of a day, because they are characterized with relatively more spatial variability among others for RCP4.5 emission scenario results [8].

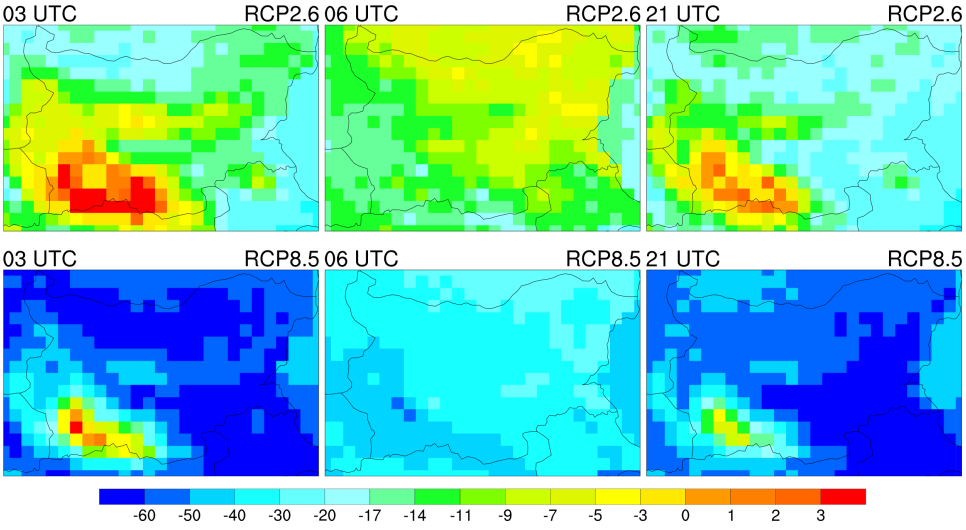

Figure 2: Differences of the yearly-average number of cases with "cold" UTCI categories between the RCP2.6 and RCP8.5 scenarios and the historical period.

3 Results

The distribution of the UTCI cold categories counts (fig. 1) shows a spatial and diurnal diversity. From the chosen periods, we suggest that the spatial diversity is most pronounced at early morning and in midnight hours for both of the scenarios. The smallest number of cases is simulated for 06 UTC. However, the numbers of average cases by year are bigger for the optimistic one. In the mid-morning period, the RCP2.6 scenario shows more cases in the southwestern part of the country and the Rhodopi Mountains. The biggest numbers of cases simulated in the mountain parts are bigger than in the non-mountain ones, because of the colder and windier conditions there, in comparison with the other country areas. Comparing the future scenarios and the historical one, the following features emerge. For cold UTCI cases, the differences are mostly negative (fig. 2). The RCP2.6 scenario have smaller an absolute values, change, than the ones in RCP8.5. The positive differences are simulated for 03 UTC and 21 UTC in the southern mountains and Southwestern Bulgaria. In RCP2.6, these two simulation times are characterized by more emphasized changes in the former regions, related to the other parts of the country. There is a increasing in the high parts of the mountains, mostly in Rila-Rhodopi massif with upt o 5 cases, and decreasing in the rest of the country with up to above 50 cases for the RCP8.6. For RCP2.6 the increasing of the cases is on wider area and the decreasing is up to about 15 cases per year.

4 Conclusion

The distribution of the UTCI cold categories shows a spatial and diurnal diversity most pronounced at early morning and in midnight hours for both of the scenarios. The biggest numbers of cases simulated in the mountain parts are bigger than in the non-mountain ones. The changes in the cold conditions are mostly negative and smaller for the RCP2.6 scenarios, and more similar in some southern mountain

areas. It is seen an increasing of the number of cold and freezing cases for larger emission reduction in RCP2.6 scenario, while we could suggest a substantial decreasing when there is no measures, as in RCP8.5.

Acknowledgements

The work was partially supported by the Centre of Excellence in Informatics and ICT under the Grant No BG16RFPR002-1.014-0018, financed by the Research, Innovation and Digitalization for Smart Transformation Programme 2021-2027 and co-financed by the European Union. This work has been partially supported by the National Center for High-performance and Distributed Computing (NCHDC), part of National Roadmap of RIs under grant No. D01-325/01.12.2023.

References

[1] Gadzhev G., Ivanov V., Valcheva R., Ganev K., Chervenkov H.: HPC Simulations of the Present and Projected Future Climate of the Balkan Region. Studies in Computational Intelligence 234-248 (2021) doi: 10.1007/978-3-030-55347-0_20

[2] Ivanov V., Valcheva R., Gadzhev G.: HPC Simulations of the Extreme Thermal Conditions in the Balkan Region with RegCM4. Studies in Computational Intelligence 309–324 (2021) doi: 10.1007/978-3-030-55347-0_27

[3] van Vuuren, D.P., den Elzen, M.G.J., Lucas, P.L., Eickhout, B. Strengers, B.J., van Ruijven, B., Wonink, S., van Houdt, R.: Stabilizing greenhouse gas concentrations at low levels: an assessment of reduction strategies and costs. Clim. Change 119-159 (2007) doi:10.1007/s10584-006-9172-9

[4] Riahi, K., Gruebler, A., Nakicenovic N.: Scenarios of long-term socio-economic and environmental development under climate stabilization. Techn. Forecasting and Social Change 887–935 (2007)

[5] Bröde, P., Fiala, D., Błażejczyk, K., Holmér, I., Jendritzky, G., Kampmann, B., Tinz, B., Havenith, G.: Deriving the operational procedure for the Universal Thermal Climate Index (UTCI). International journal of biometeorology 481–494 (2012) doi: 10.1007/s00484-011-0454-1

[6] Brecht, B. M., Schädler, G., Schipper, J. W.: UTCI climatology and its future change in Germany – an RCM ensemble approach. Meteorologische Zeitschrift 153–169 (2020) doi: 10.1127/metz/2020/1010.

[7] Hynčica M., Novák M., Procházková S.: Trends and Climatology of UTCI in the Czech Republic. Environmental Sciences Proceedings (2023) doi: /10.3390/environsciproc2023026031

[8] Ivanov V., Gadzhev G. Georgieva I.: Projection of thermal sensation for RCP4.5 scenario over Bulgaria, Cybernetics and Information Technologies (2026)

* * *

Compact Finite Difference Schemes for Nonlinear Shear Wave Models in Hyperelasticity

M. Koleva, L. Vulkov

In this work, we use the Finite Difference Method (FDM) for efficient numerical solution of a quasi-linear hyperbolic equation describing nonlinear shear wave propagation in hyperelastic materials. Following a brief overview of Love-type waves in such media, the investigation focuses on the cubic Yeoh model.

The theory of wave propagation in linearly elastic media is well established, relying on the assumption of a linear stressstrain relation, and constitutes a fundamental component of seismology. The corresponding seismic wave equation is

$$\rho\frac{\partial^2 u^i}{\partial t^2} = (\lambda+\mu)\frac{\partial}{\partial x_i}\mathrm{div}\,\mathbf{u} + \mu\triangle u^i, \;\; \mathbf{u}(x^1,x^2,x^3) = (u^1,u^2,u^3), \tag{1}$$

where the Lame coefficients $\lambda, \mu > 0$ and the density $\rho > 0$ are constant parameters [1]. This model has been widely investigated in both theoretical studies and practical applications, see, for example, [1–3].

We study the propagation of a shear wave with displacement in the y-direction within the (x, z)-plane, see [1–4]. For this class of deformations, the principal invariants take the form

$$I_1 = I_2 = 3 + v_x^2 + v_z^2 = 3 + \|\text{grad}\,\mathbf{v}\|^2,$$

where the partial derivatives v_x and v_z represent the components of the shear strain. It can be demonstrated that the y-displacement v of a shear wave propagating in a generalized neo-Hookean material, characterized by the strain energy density $W = W^H(I_1)$, is governed by the following nonlinear wave equation:

$$\rho_0 v_{tt} = 2W'\left(v_x^2 + v_z^2\right)(v_{xx} + v_{zz}) + 4W''\left(v_{xx}^2 + v_{zz}^2\right)\left(v_x^2 v_{xx} + 2v_x v_z v_{xz} + v_z^2 v_{zz}\right) \tag{2}$$

The equation (2) is linear precisely when $W'' = \partial^2 W(I_1)/\partial I_1^2 = 0$, that is, when W depends linearly on the invariant $I_1 - 3$. This situation corresponds to Mooney-Rivlin materials with strain energy density $W^H = a(I_1 - 3)$. In this case, the Youngs modulus is equal to a, and equation (2) simplifies to the linear wave equation of the form (1), namely

$$\rho_0 v_{tt} = 2a(v_{xx} + v_{zz}).$$

A strain energy density function for rubber-like materials is proposed in [5] in the following form:

$$W^H = \mu(I_1 - 3) + \frac{1}{2}M(I_1 - 3)^2 + \frac{1}{3}A(I_1 - 3)^3, \tag{3}$$

where μ, M and A are material parameters. Substitution of the Yeoh model (3) into the general nonlinear shear wave equation (2) leads to

$$\begin{aligned}\rho_0 v_{tt} \;=\;& 2\left(\mu + M\left(v_x^2 + v_z^2\right) + A\left(v_x^2 + v_z^2\right)^2\right)(v_{xx} + v_{zz}) \\ & +4\left(M + A\left(v_x^2 + v_z^2\right)\right)\left(v_x^2 v_{xx} + 2v_x v_z v_{xz} + v_z^2 v_{zz}\right).\end{aligned}$$

The associated hydrostatic pressure is given by

$$p = 2\left(\mu + M\left(v_x^2 + v_z^2\right) + A\left(v_x^2 + v_z^2\right)^2\right) + p_0(t) + \rho_0 g Z.$$

By introducing the gradient operator $\nabla = \text{grad}\,(x, z)$, equation (2) can be rewritten in divergence form as

$$\frac{\rho_0}{2} v_{tt} = \text{div}\left(\left[\mu + M\|\nabla v\|^2 + A\|\nabla v\|^4\right]\nabla v\right),$$

where the term in brackets corresponds to the derivative W_1 computed at $\|\nabla v\|^2$.

An iterative algorithm is developed for the realization of a compact finite difference scheme with fourth-order accuracy in space and second-order accuracy in time, aimed at approximating the solution and its gradient in a one-dimensional model of finite deformations in hyperelastic materials. The stress-strain relation is governed by the strain energy density function [4], resulting in a gradient-dependent constitutive law.

Numerical results for nonlinear Love wave problems are provided and analyzed.

References

[1] Pioletti, D.P., Rakotomanana, L.R.: Non-linear viscoelastic laws for soft biological tissues, European Journal of Mechanics-A/Solids, vol. 19, no. 5, pp. 749759, 2000

[2] Ciarlet, P.G.: Mathematical Elasticity. Volume 1: Three-dimensional Elasticity, vol. 20 of Studies in Mathematics and its Applications. Amsterdam: Elsevier, 1988.

[3] Graff, K.F.: Wave Motion in Elastic Solids. Courier Corporation, 2012.
[4] Marsden, J. E.,Hughes, T.J.R.: Mathematical Foundations of Elasticity. Dover, 1994.
[5] McAdam, S.S.C., Agyemang, S.O., Cheviakov, A.: Nonlinear incompressible shear wave models in hyperelasticity and viscoelasticity frameworks, with applications to love waves. Wave Motion 132 (2025), 103434.
[6] Yeoh, O.H.: Some forms of the strain energy function for rubber. Rubber Chemistry and technology 66(5) (1993), 754–771.

* * *

Mixed Precision Non-Overlapping BURA Domain Decomposition Preconditioning

N. Kosturski, S. Margenov, Y. Vutov

The performance of a non-overlapping domain decomposition (DD) preconditioner for finite element method (FEM) discretization of the Poisson equation is studded. The ParMETIS library is used to partition the mesh into sub-domains. $\Omega_i, i = 1, 2, \ldots, p$ with interface γ.

For the preconditioning of the obtained linear system, a block factorization of the matrix A is used. The blocks correspond to the degrees of freedom internal to Ω_i and those on γ. The inverse of the Schur complement, corresponding to the unknowns on γ is approximated using the best uniform rational approximation (BURA) of order k of $\Lambda^{-1/2}$, where Λ is the discretization of the Laplace-Beltrami operator on the interface γ. The inverses of the blocks, corresponding to the unknowns internal to Ω_i can be computed without any communication.

All computations within the preconditioner are performed in single precision arithmetics, while the outer solver uses standard double precision.

Numerical experiments are presented to demonstrate the applicability and performance of the proposed approach.

Acknowledgements
This work was partially supported by the Centre of Excellence in Informatics and ICT under Grant No.BG16RFPR002-1.014-0018-C01, financed by the Research, Innovation, and Digitalization for Smart Trans formation Programme 2021-2027 and co-financed by the European Union, and by the Bulgarian National Science Fund under Grant No.KP-06-N72/2.

* * *

Error Analysis for Higher-Order Methods for Subdiffusion Equations on Quasi-Graded Meshes

N. Kopteva

An initial-boundary value problem with a Caputo time derivative of fractional order $\alpha \in (0, 1)$ is considered, solutions of which typically exhibit a singular behaviour at an initial time. I will start with a review of [1] and [2], where we give a simple and general numerical-stability analysis using barrier functions, which yields sharp pointwise-in-time error bounds on quasi-graded temporal meshes

with arbitrary degree of grading. This approach was initially employed in the error analysis of the L1 method. This methodology is also generalized for semilinear fractional parabolic equations [3].

The main focus of the talk will be on higher-order discretizations, such as the Alikhanov L2-1_σ scheme, also considered in [2], and an L2-type discretization of order $3-\alpha$ in time [4]. Some recent results for the latter will also be presented [5]. The theoretical findings are illustrated by numerical experiments.

References

[1] N. Kopteva, Error analysis of the L1 method on graded and uniform meshes for a fractional-derivative problem in two and three dimensions, Math. Comp., 88 (2019), 2135–2155.

[2] N. Kopteva and X. Meng, Error analysis for a fractional-derivative parabolic problem on quasi-graded meshes using barrier functions, SIAM J. Numer. Anal., 58 (2020), 1217–1238.

[3] N. Kopteva, Error analysis for time-fractional semilinear parabolic equations using upper and lower solutions, SIAM J. Numer. Anal., 58 (2020), 2212–2234.

[4] N. Kopteva, Error analysis of an L2-type method on graded meshes for a fractional-order parabolic problem, Math. Comp., 90 (2021), 19–40.

[5] N. Kopteva, Error analysis of an L2-type method on graded meshes for semilinear subdiffusion equations, Appl. Math. Lett., 160 (2025), 109306.

* * *

Anomalous Heat Diffusion in Biological Tissues: A Fractional Laplacian Approach

S. Margenov, D. Slavchev

Anomalous diffusion is observed in many natural processes and is particularly prominent in transport phenomena within living biological tissues. Modeling modern clinical treatments, such as cancer hyperthermia and cryosurgery, is therefore of significant interest. Heat transfer in biological tissues is inherently complex due to their heterogeneous structure and physiological activity. In particular, blood flow through dense capillary networks has a substantial impact on thermal transport. In this work, we employ the fractional Laplacian operator with $\alpha > 1$ to model superdiffusive heat transfer in tissues characterized by dense vascularization.

We consider the following fractional bioheat equation:

$$\rho c \frac{\partial T}{\partial t} - k l^{2(\alpha-1)} (-\Delta)^\alpha T = J \cdot E,$$

where ρ denotes the density, c the specific heat capacity, T the temperature, and t the time. The term $k l^{2(\alpha-1)}$ represents the fractional thermal conductivity, with k being the classical thermal conductivity and l a characteristic length scale. The operator $(-\Delta)^\alpha$ is the fractional Laplacian of order α, while $J \cdot E$ describes Joule heating, where J is the current density and E is the electric field.

Our goal is to determine a reasonable range of values for the fractional parameters α and l. To this end, we compare our results with those obtained from similar models that incorporate alternative representations of capillary blood flow.

Acknowledgements

This work was partially supported by the Centre of Excellence in Informatics and ICT under Grant No.BG16RFPR002-1.014-0018-C01, financed by the Research, Innovation, and Digitalization for Smart Trans formation Programme 2021-2027 and co-financed by the European Union, and by the Bulgarian National Science Fund under Grant No.KP-06-N72/2.

* * *

The Frequency Landscape of Genomic Sequences Across Organisms

I. Marqués-Campillo

The most basic descriptor in comparative genomics is the count of how often each k-letter word appears in a genome. In a recent BioSystems article (Marqués-Campillo, Arbeitman, González and Piro, 2026, doi:10.1016/j.biosystems.2025.105635), we showed that this apparently uniform list of counts hides a rich, layered structure. Working on the human reference genome at k=11 and k=12, the 4^k possible k-mers do not scatter uniformly when stratified by their genomic frequency: five independent observables — the chaos-game position of each frequency class, the local fractal dimension of the resulting point cloud, the Hamming distance between the consensus sequences of different classes, the dinucleotide composition (especially CpG) per class, and the exact compliance with Chargaff's second parity rule — vary smoothly and coherently with the underlying frequency. The result is a continuous transition between two compositional phases: a rare regime, fractal and CG-enriched, and an abundant regime, more uniform and AT-rich, with a sharp transition at a characteristic frequency near f $\approx$ 80 for 12-mers.

In this talk we extend that analysis to a multi-organism panel including Escherichia coli K-12, Mycoplasmoides genitalium, Saccharomyces cerevisiae, the bacteriophage T4, and the recently described Obelisk RNA family. We show that the frequency-stratified organisation observed in the human genome is shared across very different genomes — bacterial, fungal, viral, and non-cellular — with organism-specific variations: the CpG-vs-AT polarity of the rare-to-abundant transition reorganises in line with each species' mutational and epigenetic landscape, and the same fractal-to-uniform transition appears even in the smallest non-cellular RNA agents. The convergence suggests that frequency-stratified compositional structure is not a peculiarity of the vertebrate genome but a generic feature of biological sequences, and we close with a brief discussion of ongoing developments aimed at turning this empirical organisation into a unified framework for genome comparison.

* * *

Novel Technologies for Imaging, Mapping and 3D Modeling of Underground Archaeological and Karst Objects – a Medieval Well in Greben Mountain and a Karst Complex near Karlukovo Village, West Bulgaria

T. Ostromsky, P. Georgiev, G. Vasilev, G, Evtimov, M. Raykovska, S.-M. Gurova

Abstract

Recent advances in remote sensing and digital documentation have significantly improved the investigation and preservation of underground archaeological and karst environments. This study presents an integrated methodological framework combining terrestrial LiDAR scanning, close-range photogrammetry, and marker-based spatial control for high-resolution 3D imaging, mapping, and modeling of

complex subterranean objects. LiDAR technology enables the acquisition of dense and geometrically accurate point clouds, even in low-light and morphologically complex environments, while photogrammetry contributes detailed texture information and complements areas inaccessible to laser scanning.

The proposed approach is applied to two case studies in Western Bulgaria: a medieval well located in Greben Mountain, in the vicinity of the village of Garlo, Breznik municipality, and a part of the famous karst complex in the vicinity of Karlukovo Village, Lukovit municipality. These sites are quite different in nature, posing various challenges to their explorers, including limited accessibility, complex and irregular geometry, high humidity and very large differences in lighting. Another common constraint in both cases is the absence of natural reference points. To deal with it, a system of dedicated artificial markers was implemented, ensuring accurate coregistration and scaling of heterogeneous datasets.

The results demonstrate that the integration of LiDAR and photogrammetric techniques allows the generation of precise, high-resolution 3D models suitable for spatial analysis, conservation planning, and virtual visualization. The methodology reduces subjectivity in documentation and enhances the reproducibility of archaeological interpretations, in line with current trends in non-destructive heritage investigation. Furthermore, the study highlights the potential of such technologies for multidisciplinary applications, including speleology, geomorphology, and cultural heritage management.

The presented work contributes to the development of efficient and adaptable digital documentation strategies for underground environments, offering prospects for large-scale, non-invasive exploration and long-term preservation of complex archaeological and karst systems.

Keywords: Photogrammetry, LiDAR, Archaeology, Speleology, Karst, Cave

1 Introducton

Karst terrains, together with their caves and vertical shafts, constitute some of the most intricate and scientifically significant geological environments on Earth. They host a wide variety of unique mineral formations, complex hydrogeological systems, and highly sensitive ecosystems. Underground karst systems, in particular, attract considerable attention not only in fundamental disciplines such as geology and speleology, but also in applied domains including natural hazard assessment, groundwater resource management, cultural heritage conservation, and sustainable tourism development. Despite their importance, many subterranean structures remain only partially explored, while some of the most challenging sections are still entirely unknown.

The detailed investigation and documentation of such environments have long been hindered by the inherent difficulties of working underground. Confined spaces, complete absence of natural light, irregular geometries, high humidity, and limited accessibility pose serious technical and safety constraints. Traditionally, speleological mapping has relied on methods such as tape-and-compass surveys, planimetric sketches, and total-station measurements. While these techniques have played a fundamental role in cave exploration for decades, they are often labor-intensive, susceptible to cumulative errors, and inadequate for capturing the full three-dimensional complexity of karst systems. As a result, they fall short of providing the level of detail and accuracy required for modern analytical, conservation, and visualization purposes.

In response to these limitations, the demand for precise, high-resolution, and reproducible digital representations has stimulated the adoption of advanced imaging technologies. Among them, LiDAR (Light Detection and Ranging) and photogrammetry have emerged as particularly powerful and complementary tools. Terrestrial Laser Scanning (TLS) enables the rapid acquisition of dense and geometrically accurate point clouds, capable of representing even highly irregular cave morphologies with millimetric precision. Photogrammetric approaches contribute detailed surface textures and allow the documentation of areas that are difficult to access with larger scanning equipment. When integrated into a unified workflow, these techniques facilitate the creation of highly realistic and metrically reliable digital twins

of underground objects comprehensive 3D models suitable for scientific analysis, long-term archiving, and immersive visualization.

2 Case study: Svirchovitsa Cave, Karlukovo village

An illustrative example for the application and evaluation of such methodologies is Svirchovitsa Cave, located near the village of Karlukovo in Northwestern Bulgaria. The cave lies within the Kamenopole Karlukovo karst region, one of the most prominent karst areas in the country, in close proximity to the Iskar Gorge and the well-known Prohodna Cave, famous for its monumental entrance and the characteristic eye-like openings in its ceiling.

Svirchovitsa Cave is distinguished by a complex internal structure, comprising multiple levels, horizontal passages, vertical shafts, and cascade-like sections, as well as chambers rich in speleothems. These characteristics make it both a demanding object of study and an ideal natural laboratory for testing the effectiveness and limitations of integrated LiDAR photogrammetric workflows under real underground conditions. The results obtained from such case studies contribute not only to improved documentation practices but also to the broader development of non-invasive, high-precision methods for the exploration and preservation of karst environments.

3 Case study: Medieval well Garlo in Greben Mountain

Another test site for the application of advanced 3D imaging and mapping techniques is the medieval well, located in Greben Mountain, in the vicinity of the village of Garlo (Breznik Municipality, Western Bulgaria) and often called by the same name. Unlike natural karst caves, this object represents a man-made subterranean structure, likely associated with medieval settlement activity, and therefore introduces a different set of geometrical, material, and interpretative challenges.

The well is characterized by a vertical shaft, about 6 m deep, relatively wide at the upper part. ? descending tunnel with stairs leads from the surface to a spacious circular plate around the well, with limited natural illumination. The well continues in depth with smaller diameter. Its internal structure is made by irregular stone lining, partial collapses occur. From a methodological perspective, such unstable and predominantly vertical environments are particularly demanding, as they restrict ground-based scanner positioning, reduce line-of-sight coverage, and introduce shadow zones in both LiDAR and photogrammetric datasets. Therefore, a drone-based photogrammetry was essential for complete 3D modeling of this object.

4 Conclusions

Traditional documentation approaches, such as manual depth measurements, sketch-based recording, or single-point surveying, are insufficient for capturing the full spatial complexity and structural condition of some underground natural objects or ancient constructions. Safety concerns related to vertical access, instability of the walls, further limit the applicability of conventional techniques.

The combined use of terrestrial LiDAR, aerial and close-range photogrammetry, supported by a system of dedicated markers, offers a robust solution to these challenges. LiDAR scanning enables the acquisition of precise geometric data on the walls of the shaft, while photogrammetry contributes high-resolution texture information, essential for documenting construction details, masonry patterns, and potential archaeological features. The use of artificial control points ensures accurate alignment between multiple scans and image sets, particularly important in environments where natural reference features are scarce.

Acknowledgement
This work is supported in parts by the Bulgarian National Science Fund via the projects Integrated System for Sustainable Research of Rock Complexes and Underground Cavities through Digital Twins, contract KP-06-N92/1 and Integrated approach to creating digital twins of archaeological immovable monuments using innovative technologies, contract KP-06-N82/1. The work of Silvi-Maria Gurova was partially supported by the Centre of Excellence in Informatics and ICT under the Grant No BG16RFPR002-1.014-0018-C01, financed by the Research, Innovation and Digitalization for Smart Transformation Programme 2021-2027 and co-financed by the European Union. We acknowledge also the access provided to the E-Infrastructure of the Laboratory for 3D Digitization and Microstructural Analysis at the Institute of Information and Communication Technologies, Bulgarian Academy of Sciences, Grant No BG05M20P001-1.001-0003.

References
[1] Antinozzi, S., di Filippo, A., Musmeci, D. (2022). Immersive Photographic Environments as Interactive Repositories for Preservation, Data Collection and Dissemination of Cultural Assets. In: Heritage, Vol. 5(3), pp. 1659-1675.
[2] Georgiev, P. Y., Prahov, N., Dimitrov, L. & Prodanov, B. (2021). Underwater non-destructive survey in connection with a project for "Multidisciplinary research of the Burgas bay - MIDBAY", Archaeological DIscoveries and Excavation in 2020, I, pp.108-113.
[3] Higuera-Trujillo, J. L., Maldonado, J. L. T., Millán, C. L. (2017). Psychological and physiological human responses to simulated and real environments: A comparison between Photographs, 360 Panoramas, and Virtual Reality. In: Applied ergonomics, Vol. 65, pp. 398-409.
[4] Ostromsky Tz., Raykovska M, Kabadzhova Ch., Petkov N., Georgiev P. (2025). Application of LiDAR and Photogrammetric Technologies for Imaging, Mapping and 3D Modeling of Underground Karst Objects - Results from Experiments in Svirchovitsa Cave near Karlukovo Village, NW Bulgaria. Journal of Physics: Conference Series, Vol. 3145 (1), IOP Publishing, ISSN:1742-6596, DOI:10.1088/1742-6596/3145/1/012004
[5] Ratcliff, T., 2010. A World in HDR. New Riders.
[6] Starkova, L. (2020). Toward a High-Definition Remote Sensing Approach to the Study of Deserted Medieval Cities in the Near East. In: Geosciences, Vol. 10 (9), 369, pp. 2-20.
[7] Supinsky, J., Pavelka, K., & Matouskova, E. (2022). Processing LiDAR point clouds for large-scale cave mapping: Methods and challenges. International Journal of Speleology, 51(1), 4558. https://doi.org/10.5038/1827-806X.51.1.2452.
[8] Vasilev, G. , Klecherova, H. , Evtimov, G. , Raykovska, M. , Petrova, V., Georgiev, I. Comprehensive digitization of the "Kazlacha" circular enclosure complex: an adaptive synergistic approach. Studies in Computational Intelligence, Springer Verlag, ISSN:1860-949X (to appear)

* * *

On the Stability of β-Sheet Inhibitors for PD-L1: Insights from REMD

X. Peng

Designing stable β-sheet inhibitors for protein-protein interactions remains challenging because isolated peptides tend to lose their secondary structure. Using replica exchange molecular dynamics (REMD), we investigate four PD-L1-targeting peptides (EE, EH, EI, ES) designed by an amino acid side-chain engineering (AASE) strategy, where EE is the lead peptide and EH/EI/ES are variants with optimized side-chain interactions. We find that side-chain interlocking — a cooperative network of complementary electrostatics, interchain hydrogen bonds, and π-π stacking — is the key to β-sheet stability. Dimer simulations show that EH forms a stable antiparallel β-sheet with up to 11 interchain hydrogen bonds and a minimum potential energy of -449.3 kJ/mol, while EE is destabilized by like-charge repulsion. EI and ES show intermediate stability. Trimer simulations and temperature-dependent analyses

further confirm EH's stability. This work establishes side-chain interlocking as a design principle for stable β-sheet PPI inhibitors.

* * *

Super-Resolution Reconstruction of Satellite Data: Validation and Uncertainty Assessment for Earth Observation Applications

E. Panek-Chwastyk, K. Dabrowska-Zielińska

Super-resolution reconstruction has emerged as a powerful approach for enhancing the spatial resolution of satellite imagery, enabling the extraction of fine-scale information beyond native sensor capabilities. However, increasing spatial resolution through data-driven or model-based reconstruction raises fundamental questions regarding the fidelity and reliability of the resulting data, particularly in the context of quantitative Earth observation applications.

In this talk, I will focus on the validation and uncertainty assessment of super-resolution reconstruction applied to satellite data. The study investigates the impact of resolution enhancement on the spectral consistency of reconstructed images, addressing the hypothesis that super-resolution methods may introduce distortions that affect the physical interpretability of observed signals. A reconstruction approach developed by Gamma Earth is considered, enabling up to a tenfold increase in the spatial resolution of Sentinel-2 imagery (from 10 m to approximately 1-2 m).

The proposed framework combines application-oriented calibration with quantitative validation strategies, including comparisons with reference data and evaluation across multiple use cases. The calibration process involves adapting reconstruction models to specific domains, with the aim of reducing systematic errors and improving the analytical value of the enhanced data. Particular attention is given to uncertainty assessment and the propagation of reconstruction-induced errors in downstream analyses.

The methodology is evaluated across three application domains: precision agriculture, energy infrastructure monitoring, and urban management. The results demonstrate how domain-specific calibration improves the reliability of super-resolved products and supports their integration into decision-making workflows.

* * *

Application of Differential Topology to Matrix Analysis

P. Petkov

This talk describes the application of methods from differential topology to several basic problems in matrix analysis. In particular, it focuses on the use of smooth manifolds and smooth mappings to study fundamental issues such as identifying singular sets, determining matrix rank, and computing the Jordan form in the presence of uncertainties. It is shown that the efficient solution of matrix problems in the presence of uncertainties involves the application of regularization techniques based on projection onto higher–codimension strata.

In this talk we describe the application of methods from differential topology to several basic problems in matrix analysis. In particular, we focuse on the use of smooth manifolds and smooth mappings to

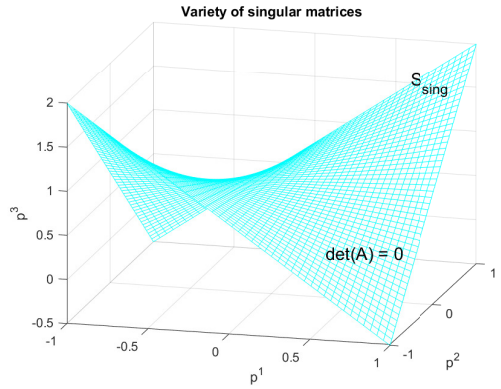

Figure 1: Variety of 4×4 singular matrices in the three-dimensional parameter space

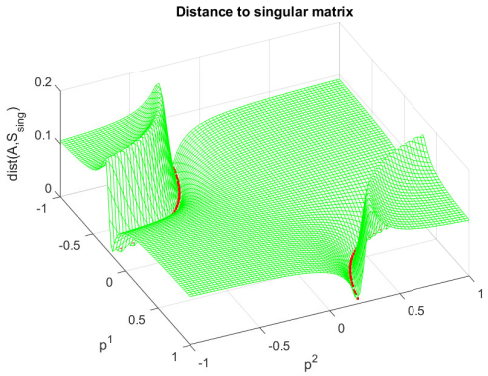

Figure 2: Distance of matrices with $(p^1, p^2) \in \mathbb{R}^2$ and $p^3 = 1$ to the variety of singular matrices

study fundamental issues such as identifying singular sets, determining matrix rank, and computing the Jordan form in the presence of uncertainties. Several examples are provided to illustrate these concepts and their practical relevance.

1 Geometry of Matrix Space

1.1 Generic and Well–Posed Problems

Example 1. *Consider a 4×4 matrix whose entries are functions of the parameters p^1, p^2, p^3. The set of singular problems represents a hypersurface of dimension 2 and codimension 1 in the three-dimensional parameter space (Fig. 1). All points outside $\mathcal{S}_{\text{sing}}$ correspond to matrices A that are nonsingular.*

1.2 Conditioning and Distance to an Ill–Posed Problem

Example 2. *Consider a 4×4 parameter–dependent matrix A depending on the three parameters p_1, p_2 and p_3. Figure 2 shows the distance in the parameter space from the matrices lying in the plane $(p^1, p^2) \in \mathbb{R}^2$, $p^3 = 1$, to the manifold $\mathcal{S}_{\text{sing}}$ of singular matrices.*

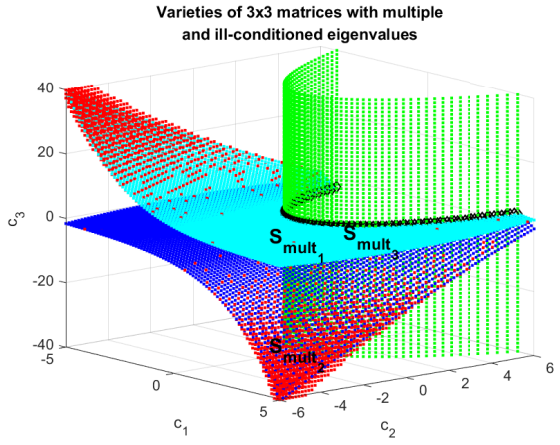

Figure 3: Matrices with poorly conditioned simple eigenvalues (shown as red dots) in the neighborhoods of the manifolds of 3×3 matrices with multiple eigenvalues

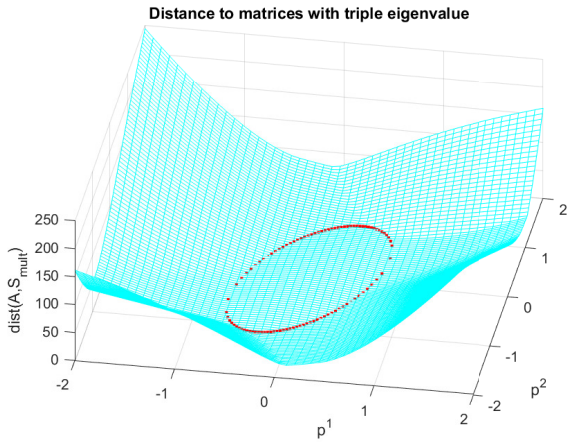

Figure 4: Distance from matrices with $(p^1, p^2) \in \mathbb{R}^2$, $p_3 = 0$ to the variety of matrices with triple eigenvalue $\lambda_1 = \lambda_3 = \lambda_4$ as a function of parameters p^1 and p^2

Example 3. *Consider the set of* 3×3 *matrices. In Fig. 3, the red dots represent* 3×3 *matrices whose maximum eigenvalue condition number exceeds 15. It can be seen that these matrices lie in the neighborhoods of the varieties of matrices with multiple eigenvalues.*

Example 4. *Figure 4 shows the distance in the parameter space from matrices lying in the plane* $(p^1, p^2) \in \mathbb{R}^2$, $p^3 = 0$, *to the manifold* $\mathcal{S}_{\mathrm{mult}_{3,4}}$ *of matrices with a triple eigenvalue as a function of the parameters* p^1 *and* p^2.

2 Geometry of Matrix Rank

The manifold defined as

$$\mathcal{O}(A) = \{PAQ^{-1} : \det(P)\det(Q) \neq 0\}, \tag{1}$$

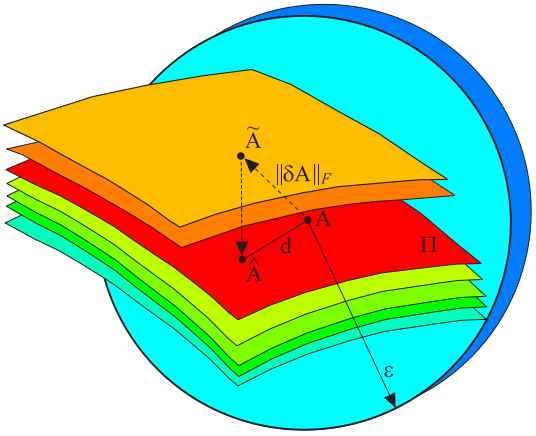

Figure 5: Determining the numerical Jordan form

is called the ***orbit*** of A. Since equivalent transformations preserve the rank of a matrix, each orbit consists of all matrices of a fixed rank r and the entire space $\mathbb{C}^{m\times n}$ is partitioned into orbits containing matrices of the same rank.

Theorem 1. *The codimension of the set of rank–r matrices in $\mathbb{C}^{m\times n}$, that is, the dimension of the normal space $N_A\mathcal{O}(A)$ in $\mathbb{C}^{m\times n}$ is*

$$\operatorname{codim}(\mathcal{O}(A)) = (m-r)(n-r).$$

Theorem 2. *In the matrix space $\mathbb{C}^{m\times n}$, the orbit $\mathcal{O}_r$ of matrices of rank r is contained in the closure of the orbit $\mathcal{O}_s$ if and only if $r \le s$ or, equivalently,*

$$\operatorname{codim}(\mathcal{O}_r) \ge \operatorname{codim}(\mathcal{O}_s).$$

More precisely,

$$\overline{\mathcal{O}}_0 \subseteq \overline{\mathcal{O}}_1 \subseteq \cdots \subseteq \overline{\mathcal{O}}_{\min\{m,n\}}.$$

3 Geometry of Jordan Form

Definition 1. *Let $A \in \mathbb{C}^{n\times n}$ and let $\varepsilon > 0$. Suppose that an approximation*

$$\widetilde{A} = A + \delta A$$

of A is given, where $\|\delta A\|_2 < \varepsilon$. Let $\Pi \subset \mathbb{C}^{n\times n}$ be a matrix bundle such that

$$\operatorname{codim}(\Pi) = \max\{\operatorname{codim}(\Pi') \colon \operatorname{dist}(\widetilde{A}, \Pi') < \varepsilon\} \tag{2}$$

and let $\widehat{A} \in \Pi$ be a matrix satisfying

$$\|\widehat{A} - A\|_2 = \min_{B\in\Pi}\|B - A\|_2$$

*with exact Jordan decomposition $\widehat{A} = ZJZ^{-1}$. Then the matrix J is called the **numerical Jordan canonical form** of A within ε, and ZJZ^{-1} is called the **numerical Jordan decomposition** of A within ε.*

* * *

Proactive Fuzzy-ACO Framework for Resilient Outsourced Production

J. Stanchov, S. Fidanova

In the era of Industry 4.0, decentralized garment manufacturing requires a paradigm shift from reactive to proactive scheduling. The integration of internal knitting operations with volatile external subcontractor networks necessitates an intelligent, risk-aware framework. To harmonize these processes, we propose a Proactive Fuzzy-ACO system.

The problem is modeled as a Hybrid Flow-shop Scheduling Problem (HFSP) integrated with a Capacitated Vehicle Routing Problem (CVRP), where we define a Pareto-optimal solution set by minimizing the objective vector $\text{vec}F = [f_1, f_2, f_3]$.

The first objective, f_1, minimizes total tardiness, while the second objective, f_2, minimizes the economic impact. Finally, systemic risk is addressed by f_3, ensuring the avoidance of unreliable nodes within the subcontractor network. The interaction between these variables is governed by the Dual-Trail ACO engine, allowing the system to balance logistics efficiency against stochastic disruption risks in real-time.

Computational simulations demonstrate that the proposed Fuzzy-ACO framework effectively navigates the multi-objective optimization landscape (Fig. 1).

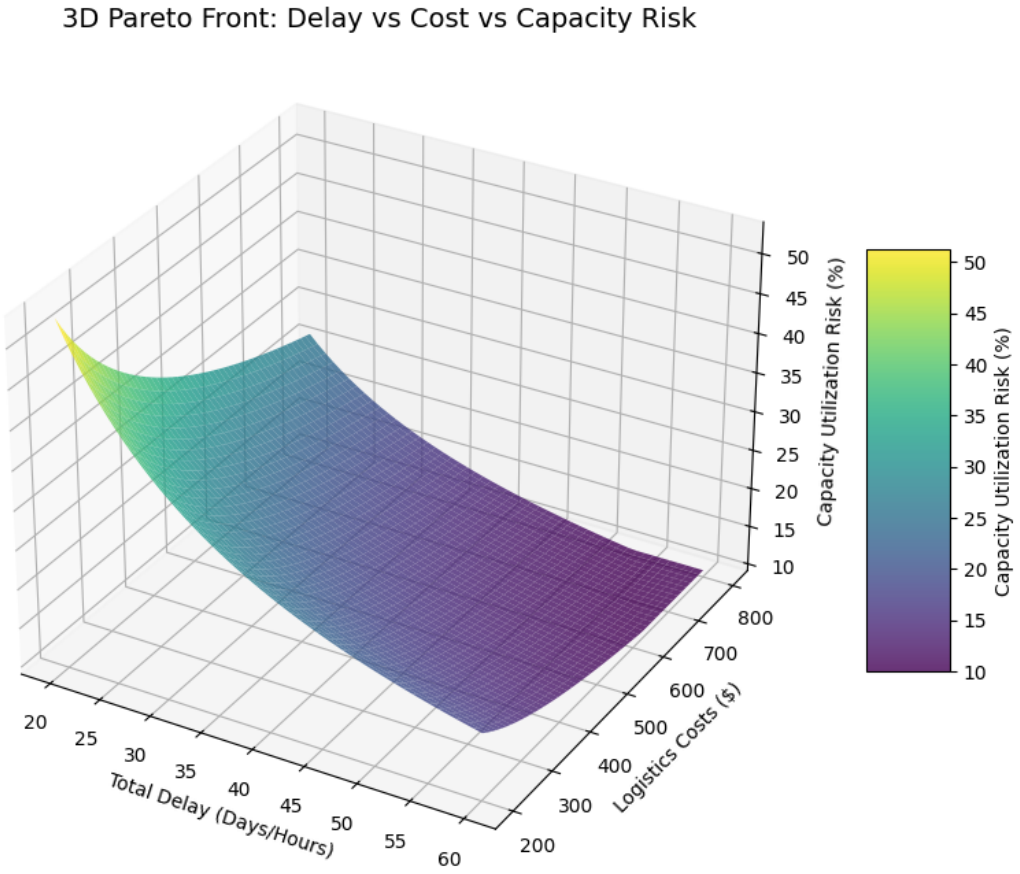

Figure 1: 3D Pareto Front Analysis: Interaction between financial cost, temporal efficiency, and fuzzy subcontractor capacity risk.

The 3D surface highlights an ”optimal trough” where the system balances total delay and logistics costs while maintaining capacity utilization risk within defined thresholds. Unlike traditional reactive

models, the proactive strategy utilizes real-time fuzzy signals to prevent high-risk configurations. Quantitative analysis confirms that this approach delivers a 42% improvement in cost-resilience efficiency, successfully mitigating potential production disruptions.

This study introduces a risk-aware, proactive scheduling framework that bridges the gap between theoretical metaheuristic optimization and the stochastic nature of decentralized manufacturing. Future efforts will extend this framework by incorporating real-time IoT streams and sustainability metrics to develop a comprehensive "Green Resilience" model.

Keywords: Dynamic Scheduling, Ant Colony Optimization (ACO), Fuzzy Logic, Resilient Manufacturing, Rolling Horizon Strategy, Outsourced Production, Pareto Optimization.

Acknowledgment

The work was partially supported by the Centre of Excellence in Informatics and ICT under the Grant No BG16RFPR002-1.014-0018-C01, financed by the Research, Innovation and Digitalization for Smart Transformation Programme 2021-2027 and co-financed by the European Union.

* * *

MolSim++: GPU Confined Particle Dynamics Project

J. Thacker, I. Todorov, B. Speake, M. Seaton

We present a new particle dynamics driver (to address Dissipative Particle Dynamics and Molecule Dynamics simulation) aimed at performing on GPU architectures while extensible to future hardware advances. Embodying best software practices, the project was conceived in C++ and adopts the SYCL standard to leverage GPU parallelism while also being vendor and compiler agnostic. We will present the project evolution, the core algorithms underpinning our GPU confined performance and compare our performance to that of other leading particle dynamics engines' GPU ports (e.g, LAMMPS-kokkos and GROMACS-CUDA). We will discuss various aspects of our strategy to balance performance gains and compromises on a GPU, the performance-portability of SYCL kernels, and how our project strives to maximise code reuse and sustainability by adopting core software design principles. We will also outline the benefits and consequences of starting a software project from scratch (as opposed to building upon our previous software experiences DL_POLY, DL_MESO and their CUDA ports).

* * *

Polarised Water Model for CG DPD Simulations of RFB Electrolytes

I. Todorov, M. Seaton, B. Speake

The talk will highlight our progress in the area of designing and applying coarse-grained (CG) Dissipative Particle Dynamics (DPD) interaction for mesoscopic simulations of water. Mesoscopic models have gained popularity as they help utilise particle dynamics technologies at scales closer to continuum-based models and to real-life experiments. However, their ability to represent e.g. thermodynamic and transport properties at those scales hinges on the compromises made for the sake of computational performance, which unfortunately often integrate out critical information from well-established atomistic

models. In our studies we have critically evaluated these inevitable losses through iterative coarse-graining procedures, starting from high quality atomistic models, and demonstrated how crucial it is to account for and capture the dualistic nature of the mesoscopic scale. The ability to polarise CG liquids is especially relevant for polar solvents such as water, since these require effective representation of their dielectric nature as driven by molecular charge distributions and molecular network structuring. The dielectric nature of a medium leads to complex phenomena such as local polarisability response and restructuring near interfaces in reaction to changes in local charge distributions. Inclusion of such phenomena when using larger-than-atomistic techniques such as coarse-grained molecular dynamics (CG-MD) and dissipative particle dynamics (DPD) is still an open question. We have polarised our originally apolar, n=4DPD 5:1 water model by using an internal 3-site charge distribution and demonstrated the emerging dielectric behaviours. A number of key dielectric properties were validated against those from the CG "ground truth" atomistic water model (TIP3P-RM) and compared against those from other polar CG water models, also tuned to reproduce atomistic water dipole distributions. Our own model not only performs better than the existing alternative approaches but also allows for a medium quadrupole as well as for a steady linear dielectric response to much higher external electric fields. Our best polar water model is now actively used for modelling Vanadium based RFB electrolytes.

* * *

A Unified and Automated Workflow for Multi-Scale Simulation of Covalent Protein–Ligand Complexes

S. Zhao, J. Meng, X. Peng, J. Dai, Q. Zhao

Modeling protein–ligand systems, particularly those involving covalently bound chromophores, remains a complex and labor-intensive process requiring the integration of heterogeneous tools across multiple scales. Existing workflows often involve substantial manual intervention, limiting reproducibility and scalability. This challenge is especially pronounced in fluorescent protein systems, where accurate prediction of structural and spectroscopic properties requires consistent treatment of protonation states, local environments, and quantum mechanical effects.

In this work, we present an automated, end-to-end computational pipeline for multi-scale modeling of covalent protein–ligand complexes. Starting from SMILES strings and protein sequences or structures, the pipeline integrates cheminformatics tools, force-field parameterization, protein structure prediction or retrieval, and structure preparation using Rosetta, including pH-dependent protonation and explicit water placement. The prepared systems can then be seamlessly propagated to molecular dynamics simulations and quantum chemical calculations for spectroscopic analysis.

We demonstrate the capability of the pipeline on multiple fluorescent protein systems. For a protein–chromophore complex (PDB ID: 7MFX), the pipeline successfully reproduces distinct conformational states associated with different protonation conditions, consistent with experimentally observed structures. For avGFP and eGFP systems, starting from predicted structures, subsequent structural refinement and quantum chemical calculations yield absorption maxima within 10 nm of experimental values. Furthermore, the pipeline accurately captures spectral shifts in mutated systems sharing the same chromophore but differing in protein environments. These results highlight the ability of the proposed workflow to enable physically consistent and reproducible multi-scale simulations, while significantly reducing manual effort. The pipeline provides a generalizable framework for studying complex covalent protein–ligand systems and is made available as an open-source tool.

Keywords: Covalent Protein–Ligand Complexes · Multi-Scale Simulation · Fluorescent Protein

* * *

RF vs. LSTM for Multi-Horizon Urban Air Quality Forecasting: A Head-to-Head Benchmark on a Calibrated Hybrid Sensor Network

P. Zhivkov

Operational air quality prediction at sub-day horizons underpins public health advisories, traffic management, and industrial scheduling in urban areas. Most published forecasting benchmarks draw on a single reference station or a small co-located cluster; the spatial heterogeneity of urban pollution goes largely uncharacterised, and evaluations on uncalibrated low-cost sensors conflate sensor error with forecast error. This study uses a different starting point: 22 spatially distributed low-cost sensors cross-calibrated against five official reference stations, providing a city-wide training signal that single-station studies cannot replicate.

Data come from Sofia, Bulgaria (population 1.3 million), recorded at hourly resolution across 24 months (August 2023 – July 2025). Each hourly observation is represented by seven input features: calibrated pollutant concentration, temperature, atmospheric pressure, relative humidity, hour of day, month, and a weekend indicator. This feature set captures both meteorological mixing conditions and anthropogenic emission timing. Concentrations were pre-calibrated using a machine-learning transfer framework described in a companion study, reducing the 30–50% systematic bias typical of raw low-cost sensors to near-reference accuracy; average data availability exceeded 96.9% across all 22 units, yielding approximately 1.2 million usable hourly records.

The Random Forest (RF) model uses an ensemble of 100 decision trees trained with bootstrap sampling and random feature subsets (maximum depth 10; minimum 10 samples per leaf). Rather than processing the raw time series, RF operates on a compact lag feature vector derived from the 24-hour lookback window: the most recent concentration, the 5-step lag (half-day diurnal shift), the 23-step lag (same-hour-yesterday), plus the window mean and standard deviation and the meteorological and temporal features at the last timestep.

The Long Short-Term Memory (LSTM) network takes a fundamentally different approach, processing the full 24×7 input matrix directly so the recurrent layer can learn temporal patterns without manual feature engineering. The architecture consists of a single 32-unit LSTM layer, a Dropout layer ($p = 0.2$) for regularisation, a 16-unit dense layer with ReLU activation, and a linear output; approximately 5,700 trainable parameters in total. Training uses the Adam optimiser (learning rate 10^{-3}), batch size 128, and early stopping with patience 15 epochs. Both RF and LSTM were trained on 20,000 randomly sampled sequences from the pooled 22-sensor dataset (roughly 38 days of network-wide data) under an identical budget, ensuring a fair, directly comparable evaluation.

Several aspects distinguish this work from existing benchmarks. Training sequences are pooled from all 22 sensors; this spatial aggregation exposes both models to the full range of urban microenvironments in the network, rather than constraining them to a single station's temporal record. The calibration and forecasting problems are kept separate by design: sensor accuracy is established in a companion paper, and only the resulting verified concentrations serve as model inputs here. The study also reveals a consistent, interpretable pollutant-dependent performance split. RF's lag feature structure aligns naturally with the regular diurnal NO_2 traffic cycle; LSTM's sequential context provides incremental benefit for O_3 at longer horizons, where photochemical dynamics depend on solar angle and boundary-layer history that a handful of lag values cannot fully encode.

Across all nine pollutant–horizon combinations (PM_{10}, NO_2, O_3 at 1 h, 6 h, and 24 h), RF and LSTM are closely matched; no pairwise R^2 difference exceeds 0.04. The 6-hour horizon is operationally the

most revealing: persistence fails for all three pollutants (R^2 as low as -1.66 for NO_2), while both ML methods maintain positive skill ($R^2 = 0.45$–0.79). At 24 hours, RF leads for PM_{10} and NO_2; LSTM edges ahead for O_3. RF skill proves stable across Spring and Summer for NO_2 and O_3, suggesting the learned diurnal patterns generalise within the photochemical season.

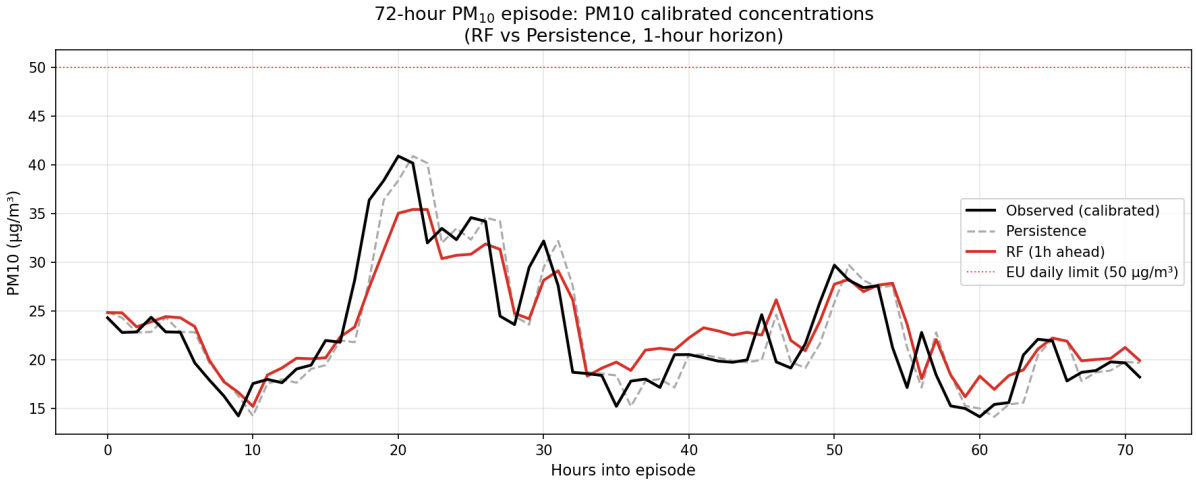

Figure 1: 72-hour PM_{10} episode: observed calibrated concentrations (black), RF 1-hour ahead forecast (red), and persistence baseline (grey dashed). The horizontal red line marks the EU daily limit (50 µg/m^3). RF anticipates concentration build-up and decline phases more accurately than persistence, which systematically lags by one time step.

For most operational scenarios, RF is the preferred deployment choice; it is deterministic, requires no GPU hardware, trains in seconds on commodity hardware, and achieves equivalent or better accuracy for PM_{10} and NO_2. LSTM is the more appropriate option when O_3 forecasting at 6 h or 24 h is a priority and GPU infrastructure is available. Either method becomes viable after roughly a single monitoring season of pooled sensor data.

Two limitations bound the scope of these conclusions. Winter heating-season performance — when Sofia's mountain-basin topography drives the most severe pollution episodes through residential biomass burning under temperature inversions — falls within the training period and is not evaluated on held-out data; this remains a priority for future study. Spatial dependencies among sensors are not modelled; graph neural network architectures that incorporate network topology could address this gap and likely improve performance during advection events.

Keywords: air quality forecasting; Random Forest; LSTM; calibrated hybrid sensor networks; low-cost sensors; Sofia; multi-horizon prediction; PM_{10}; NO_2; ozone; benchmark

Acknowledgements

This work was partially supported by the Centre of Excellence in Informatics and ICT under Grant No.BG16RFPR002-1.014-0018-C01, financed by the Research, Innovation, and Digitalization for Smart Trans formation Programme 2021-2027 and co-financed by the European Union.

* * *

Auxiliary Space Preconditioning and a Posteriori Error Estimates in Finite Element Method

L. Zikatanov

We study the relations between a posteriori error estimates and subspace correction methods viewed as preconditioners for problems in infinite dimensional Hilbert spaces. We set the stage using the Finite Element Exterior Calculus and Nodal Auxiliary Space Preconditioning. This framework provides a systematic way to derive explicit residual estimators and estimators based on local problems which are upper and lower bounds of the true error. We show the applications to discretizations of curl-curl, grad-div, Hodge Laplacian problems, and linear elasticity. For singularly perturbed H(div) and H(curl) problems, we also obtain novel parameter-independent error estimators. The only ingredients needed are: well-posedness of the problem and the existence of regular decomposition on continuous level. This is a joint work with Yuwen Li (Zhejiang University).

* * *

List of participants

L'Yazid Ait Salah
University of Béjaia
Cité Djama Béjaia
Algeria
lyazid.aitsalah@outlook.com

Joshua Bannister
Flat 19, Coriander House, 18 Colina Road
London, United Kingdom
joshua.bannister.14@ucl.ac.uk

Hitesh Bansu
R N G Patel Institute of Technology
125, Mahavirdham-2, New kosad road Amroli
Surat, Gujarat, India
hiteshbansu@gmail.com

Hristo Chervenkov
National Institute of
Meteorology and Hydrology
Tsarigradsko Shose blvd. 66
1784 Sofia, Bulgaria
hristo.tchervenkov@meteo.bg

Mateusz Chwastyk
Institute of Physics
Polish Academy of Sciences
Aleja Lotników 32/46
02-668 Warsaw, Poland
chwastyk@ifpan.edu.pl

Hristo Djidjev
Institute of Information and
Communication Technologies,
Bulgarian Academy of Sciences
Acad. G. Bonchev Str., bl. 25A
1113 Sofia, Bulgaria
hdjidjev@msn.com

Andrei Draganescu
University of Maryland
Baltimore County
1000 Hilltop Circle
Baltimore, MD, 21230, USA
draga@umbc.edu

Stefka Fidanova
Institute of Information and
Communication Technologies,
Bulgarian Academy of Sciences
Acad. G. Bonchev Str., bl. 25A
1113 Sofia, Bulgaria
stefka.fidanova@gmail.com

Georgi Gadzhev
National Institute of Geophysics,
Geodesy and Geography,
Bulgarian Academy of Sciences
Acad. G. Bonchev Str., bl. 3
1113 Sofia, Bulgaria
ggadjev@geophys.bas.bg

Silvia Grozdanova
Institute of Information and
Communication Technologies,
Bulgarian Academy of Sciences
Acad. G. Bonchev Str., bl. 25A
1113 Sofia, Bulgaria
silvia@parallel.bas.bg

Stanislav Harizanov
Institute of Information and
Communication Technologies &
Institute of Mathematics and Informatics,
Bulgarian Academy of Sciences
Acad. G. Bonchev Str., bl. 25A
1113 Sofia, Bulgaria
sharizanov@parallel.bas.bg

Hristo Hristov
Institute of Information and
Communication Technologies,
Bulgarian Academy of Sciences
Acad. G. Bonchev Str., bl. 2
1113 Sofia, Bulgaria
h.hristovrd@gmail.com

Nevena Ilieva
Institute of Information and
Communication Technologies,
Bulgarian Academy of Sciences
Acad. G. Bonchev Str., bl. 25A
1113 Sofia, Bulgaria
nevena.ilieva@iict.bas.bg

Veselin Ivanov
Faculty of Medicine,
Trakia University
Stara Zagora, Bulgaria
veskoasenov@abv.bg

Natalia Kopteva
Department of Mathematics and Statistics
University of Limerick
Limerick, V94 T9PX, Ireland
natalia.kopteva@ul.ie

Nikola Kosturski
Institute of Information and
Communication Technologies,
Bulgarian Academy of Sciences
Acad. G. Bonchev Str., bl. 25A
1113 Sofia, Bulgaria
nikola.kosturski@iict.bas.bg

Elena Lilkova
Institute of Information and
Communication Technologies,
Bulgarian Academy of Sciences
Acad. G. Bonchev Str., bl. 25A
1113 Sofia, Bulgaria
elena.lilkova@iict.bas.bg

Svetozar Margenov
Institute of Information and
Communication Technologies,
Bulgarian Academy of Sciences
Acad. G. Bonchev Str., bl. 25A
1113 Sofia, Bulgaria
margenov@parallel.bas.bg

Iván Marqués-Campillo
Universitat de les Illes Balears (UIB)
Calle albarrasi, 2, 2b
Palma de Mallorca, Spain
iwmarquescampillo197@gmail.com

Tzvetan Ostromsky
Institute of Information and
Communication Technologies,
Bulgarian Academy of Sciences
Acad. G. Bonchev Str., bl. 25A
1113 Sofia, Bulgaria
ceco@parallel.bas.bg

Ewa Panek-Chwastyk
Institute of Geodesy and Cartography
Zygmunta Modzelewskiego 27
02-679 Warsaw, Poland
ewa.panek-chwastyk@igik.edu.pl

Xubiao Peng
Beijing Institute of Technology
Beijing 100081, China
xubiaopeng@bit.edu.cn

Petko Petkov
Bulgarian Academy of Sciences
15 November Str. No 1
1000 Sofia, Bulgaria
php@tu-sofia.bg

Mario Shopov
Faculty of Medicine,
Trakia University
Stara Zagora, Bulgaria

Dimitar Slavchev
Institute of Information and
Communication Technologies,
Bulgarian Academy of Sciences
Acad. G. Bonchev Str., bl. 25A
1113 Sofia, Bulgaria
dimitargslavchev@parallel.bas.bg

Jelenko Stanchov
Institute of Information and
Communication Technologies,
Bulgarian Academy of Sciences
Acad. G. Bonchev Str., bl. 2
1113 Sofia, Bulgaria
elenko.stanchov@gmail.com

Joseph Thacker
STFC Scientific Computing
Keckwick Lane
Daresbury, UK
joseph.thacker@stfc.ac.uk

Ilian Todorov
STFC Scientific Computing
Keckwick Lane
Daresbury, UK
ilian.todorov@stfc.ac.uk

Lubin Vulkov
"Angel Kanchev" Ruse University
Studentska 8 Str.
7017 Ruse, Bulgaria
lvalkov@uni-ruse.bg

Yavor Vutov
Institute of Information and
Communication Technologies,
Bulgarian Academy of Sciences
Acad. G. Bonchev Str., bl. 25A
1113 Sofia, Bulgaria
yavor@parallel.bas.bg

Siteng Zhao
Beijing Institute of Technology
Beijing 100081, China
973708642@qq.com

Petar Zhivkov
Institute of Information and
Communication Technologies,
Bulgarian Academy of Sciences
Acad. G. Bonchev Str., bl. 25A
1113 Sofia, Bulgaria
zhivkovpetar@gmail.com

Ludmil Zikatanov
Penn State University ,
Department of Mathematics
239 McAllister Bldg, Penn State
16802 State College, PA, USA
ludmil@psu.edu